Underwater Optical Sensorbot for In Situ pH Monitoring

by

John Johansen

A Thesis Presented in Partial Fulfillment
of the Requirements for the Degree
Master of Science

Approved November 2011 by the
Graduate Supervisory Committee:

Deirdre R. Meldrum, Chair
Shih-hui Chao
Antonia Papandreou-Suppappola

ARIZONA STATE UNIVERSITY

August 2012

ABSTRACT

Continuous underwater observation is a challenging engineering task that could be accomplished by development and deployment of a sensor array that can survive harsh underwater conditions. One approach to this challenge is a swarm of micro underwater robots, known as Sensorbots, that are equipped with biogeochemical sensors that can relay information among themselves in real-time. This innovative method for underwater exploration can contribute to a more comprehensive understanding of the ocean by not limiting sampling to a single point and time. In this thesis, Sensorbot Beta, a low-cost fully enclosed Sensorbot prototype for bench-top characterization and short-term field testing, is presented in a modular format that provides flexibility and the potential for rapid design. Sensorbot Beta is designed around a microcontroller driven platform comprised of commercial off-the-shelf components for all hardware to reduce cost and development time. The primary sensor incorporated into Sensorbot Beta is an in situ fluorescent pH sensor. Design considerations have been made for easy adoption of other fluorescent or phosphorescent sensors, such as dissolved oxygen or temperature. Optical components are designed in a format that enables additional sensors. A real-time data acquisition system, utilizing Bluetooth, allows for characterization of the sensor in bench top experiments. The Sensorbot Beta demonstrates rapid calibration and future work will include deployment for large scale experiments in a lake or ocean.

TABLE OF CONTENTS

Page

LIST OF TABLES v

LIST OF FIGURES vi

CHAPTER

1 INTRODUCTION 1

1.1 Research Objectives and Introduction 1

1.2 Sensor Systems in Underwater Environments 2

1.2.1 Lake, River, and Estuary Systems 3

1.2.2 Ocean Systems 5

1.3 pH Sensing 15

1.4 Sensorbot Goals and Specifications 17

2 SENSORBOT BETA HARDWARE DESIGN 20

2.1 Design Background of Sensorbot Beta 20

2.2 Sensorbot Beta Hardware Design 21

2.3 Hardware Selection for Non-volatile Data Storage 22

2.4 Hardware Selection for Communication 24

2.5 Hardware Selection for the Microcontroller 25

2.6 Sensor Interface 27

2.7 Housing Considerations 28

2.8 Software Interface 28

CHAPTER

2.9 Length of Deployment and Size of the Unit 29

2.10 Sensorbot Beta Implementation 32

3 PH SENSORS FOR ENVIRONMENTAL MONITORING 33

3.1 Background of Sensor in Use 33

3.2 Sensor Coating 37

3.3 Testing and Calibration of Sensor 40

3.3.1 S1 Sensor Film 41

3.4 S1 Optics Selection for Sensorbot Beta 41

3.5 Optics Hardware 43

3.6 Sensorbot Beta Hardware Conclusion 44

4 SENSORBOT CHARACTERIZATION 47

4.1 Background 47

4.2 Full Calibration for Sensorbot Beta 47

4.3 Rapid Two Point Calibration for Sensorbot Beta 49

4.4 Simulated Field Deployment 51

4.5 Field Deployment 52

5 CONCLUSION 55

5.1 Summary of Results 55

5.2 Future Work 57

WORKS CITED 60

CHAPTER

APPENDIX A 68

APPENDIX B 76

LIST OF TABLES

Table Page

Table 1. Cabled observatories. 11

Table 2. Commercially available pH sensors for field deployment 17

Table 3. Non-volatile memory comparison. 23

Table 4. Cost of components for one Sensorbot Beta 46

LIST OF FIGURES

Figure Page

Figure 1. Example pH data of a water column as a time-course of a year. (Courtesy of Water on the Web, accessed at http://www.waterontheweb.org/ on September 1, 2011.) 5

Figure 2. Placement of NEPTUNE Canada and RSN. (http://www.interactiveoceans.washington.edu/file/RSN+Plan+View, Courtesy of the OOI Regional Scale Nodes program and the Center for Environmental Visualization, University of Washington) 8

Figure 3. DONET observatory. (Courtesy of Japan Agency for Marine-Earth Science and Technology accessed at http://www.jamstec.go.jp/jamstec-e/maritec/donet/about/news/20110808/)..... 10

Figure 4. Core hardware of Sensorbot Beta..... 22

Figure 5. Sensorbot Beta Labview interface..... 29

Figure 6. Average current consumption for one year of operation time..... 31

Figure 7. 3D model of Sensorbot Beta..... 32

Figure 8. Basic operation of sensor..... 34

Figure 9. (A) Absorption spectrum of S1. (B) Emission spectrum of S1. (Courtesy of Dr. Yanqing Tian of CBDA.) 36

Figure 10. Calibration curve of S1 with pKa of 7.01. (Courtesy of Dr. Yanqing Tian of CBDA.) 37

Figure 11. Calibration of S1 using spectrofluorophotometer. 41

Figure 12. LED and filter selection for Sensorbot Beta..... 43

Figure 13. Sensor hardware. 44
Figure 14. Sensorbot Beta complete block diagram 45
Figure 15. Experimental setup for Sensorbot Beta calibration. 48
Figure 16. Calibration of pH sensor S1 with Sensorbot Beta. 49
Figure 17. Calibration of pH sensor S1 with Sensorbot Beta using Two-Point Calibration..... 50
Figure 18. Benchtop Test of Lake Water with estimated pH, estimated pH with moving average filter (MAF), and actual pH..... 52
Figure 19. Field test location: Tempe Town Lake, Tempe, Arizona. 53
Figure 20. Field Test Results with raw signal and signal with moving average filter (MAF). 54
Figure 21. (A) UV LED spectrum. (B) Absorbance of pH sensor S1. (C) Sensor absorption from LED excitation for pH sensor S1. 71
Figure 22. (A) UV LED spectrum. (B) 450nm filter transmission. (C) Excitation cut from the filter for UV LED. 72
Figure 23. (A) Excitation of pH sensor S1. (B) 450nm filter transmission. (C) Photodiode spectrum. (D) Signal from photodiode. 75
Figure 24. Optical modem overview of circuit. 77
Figure 25. Picture of optical modem..... 78
Figure 26. Output of optical modem with IrDA and UART..... 79
Figure 27. Test setup of optical modem..... 80
Figure 28. Results of optical modem test..... 80

1 Introduction

1.1 Research Objectives and Introduction

The Center for Biosignatures Discovery Automation (CBDA) in the Biodesign Institute at Arizona State University led by Dr. Deirdre Meldrum is working on methods to monitor the harsh environment of the ocean and to better understand the chemical and biological systems. Existing methods of exploration have not provided a comprehensive spatial and temporal understanding of the ocean and are often limited to measurements in a single area and for a limited amount of time. The need for a more continuous and widespread observation of the seafloor has prompted new approaches to ocean exploration. One new approach is the National Science Foundation's (NSF) Ocean Observatory Initiative (OOI) Regional Scale Nodes (RSN) network led by Professor John Delaney of the University of Washington. The OOI Regional Scale Nodes will lay an underwater cable with bandwidth and power to service instruments on the ocean bottom for continuous observation of the ocean that will be connected to the World Wide Web so that students and researchers can learn about and study the ocean off the Northwest coast of the United States in real-time.

A unique approach that CBDA is taking to ocean exploration is the concept of the Sensorbot, a robot equipped with biogeochemical sensors that can work cooperatively in a swarm to monitor the ocean in real-time while relaying information to the internet. The Sensorbots are also able to recharge power via the

nodes on the RSN observatory. This is a challenging task to complete due to the difficulties of deployment coupled with the harsh conditions of extreme temperatures, toxic chemicals, and pressure that the Sensorbots must survive in for up to a year at a time. Some of the major challenges to overcome in designing the Sensorbot are power constraints, durable housing for high pressures, size limitations for cost and performance, extreme temperatures, and biofouling.

1.2 Sensor Systems in Underwater Environments

Sensorbots are a viable underwater sensor system for monitoring large volumes of water and being deployed for long periods of time. If the Sensorbots are made cheap and small enough, a fleet of hundreds or thousands of them could be deployed in large volumes of water, and are only limited by battery power for length of operation. Sensorbot systems may be expandable as more Sensorbots are introduced and existing Sensorbots are replaced. Communication systems on the Sensorbot will create a network for real-time monitoring. The network would allow the sensors to respond to each other and create a system that adapts its monitoring depending on input from the entire Sensorbot network. This system could be equipped to measure pH, dissolved oxygen, temperature, or other biogeochemical parameters in a region of interest. If one of these parameters has an abnormal reading, another Sensorbot could check on what is causing the change or poll other Sensorbots in the system to see if they are also receiving the

abnormal reading. All of this data could then be sent to a master system for logging and analysis at a later date.

1.2.1 Lake, River, and Estuary Systems

One successfully deployed freshwater sensor network is the SmartCoast system along the River Lee Co. Cork, Ireland [1–5]. The system is being developed by the Clarity Centre for Sensor Web Technologies with the goal of creating long term water monitoring solutions with emphasis on user needs for specific applications. By using a sensor network, a variety of sensors can be placed in situ along the river to monitor multiple regions of interest simultaneously. These sensors are connected in the network and are capable of triggering each other if there is an abnormal response. One example of a sensor triggering in the Smart Coast is using a camera to take a picture of a location of interest if there is a change in water level, pollution, or turbidity detected by one of the deployed sensors. The data from the camera (AXIS 212 PTZ) and the sensor is then sent back to a PC wirelessly for real-time monitoring by a user [6]. Data can then be extracted from the images and correlated with data from the sensor. This allows the system to be used as a warning system if one portion of the network warrants further investigation. Some of the sensors in the network can be setup to use Zigbee wireless communication, a radio frequency communication standard, to reduce the amount of tether required for the system and allow for remote nodes. Many of the contributions and lessons learned from

the SmartCoast system are being implemented in the River and Estuary Observatory Network (REON) [7] with support from IBM. REON is a sensor network that is being developed to monitor the Hudson River.

Another successfully deployed system is the Water on the Web (www.waterontheweb.org) that was initially deployed in Minnesota to have a network of various sensors report data taken from lakes and rivers to a single database [8]. The program was successful in collecting information from a variety of sensors such as water temperature, specific conductivity, dissolved oxygen, pH, and chlorophyll a. Several open-access online tools were created that have allowed for different ways to visualize and analyze the data. A curriculum was created with the large repository of information for educational use for anyone that has access to the internet. The project was funded by the National Science Foundation from 1997 to 2005 and has been in maintenance mode since (http://www.waterontheweb.org/ accessed on September 1, 2011). An example of the data presented on the site can be seen in Figure 1.

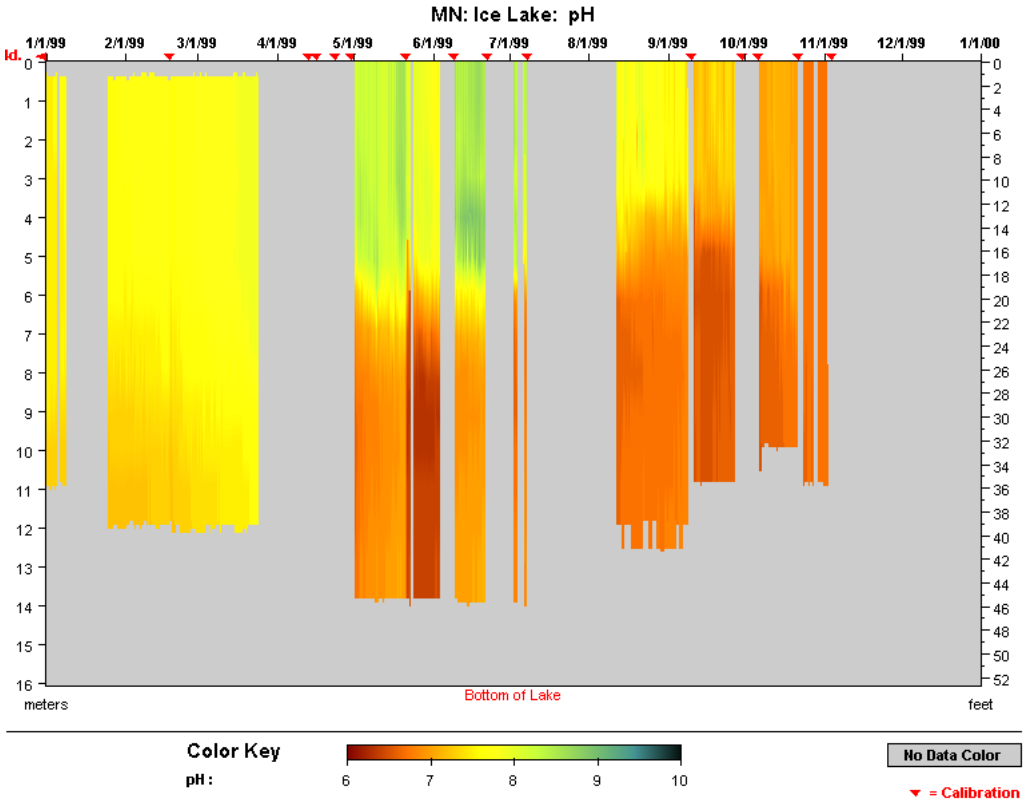

Figure 1. Example pH data of a water column as a time-course of a year. (Courtesy of Water on the Web, accessed at http://www.waterontheweb.org/ on September 1, 2011.)

1.2.2 Ocean Systems

Studying ocean systems is a difficult task that is complicated by the difficulties and cost of deployment. Scientific experiments performed just 900 kilometers from the shoreline often require larger ships, such as the *R/V Thomas G. Thompson*. Two solutions for long term ocean studies are to implement a cabled observatory and/or a network of sensors. The former is a permanent

structure that is laid on the ocean floor with the latter being a series of sensors that relay information between each other.

1.2.2.1 Ocean Cabled Observatories

Cabled ocean observatories are an important advancement in ocean science that is working to improve ocean understanding and provide a continuous presence in the ocean. A variety of systems exist for purposes such as scientific research and early earthquake warning systems. Some of these systems work independently and others are operated under an umbrella organization that coordinates a series of networks. Many of these networks have intended goals of distributing real-time data by relaying the information collected from the sensors onto the internet. This allows for many research and educational opportunities to operate year round and not be limited by power. The system can also act as a charging station for autonomous underwater vehicles (AUVs) that may be operating autonomously in the area.

There are four main cabled observatories along the western seaboard of North America: MARS (Monterey Accelerated Research System) [9–11], VENUS (Victoria Experimental Network Under the Sea) [12], [13], NEPTUNE Canada (North-East Pacific Time-Series Underwater Network Experiments) [14–17], and the RSN (Regional Scale Nodes) of the NSF Ocean Observatory Initiative [18]. Each component is placed in a location that is unique for scientific purposes. MARS is located at Moss Landing in Monterey Bay, which enters water

depths of greater than 1000 meters in a relatively short distance allowing for rapid deployment and testing of deep sea equipment. It also limits the amount of cable that needs to be laid to reach desirable depths for deep sea observation. VENUS is located in two components located at the Saanich Inlet and the Strait of George which were chosen due to their close proximity to major cities, Victoria and Vancouver, respectively. Some of the successes of VENUS include measuring the effects of Fraser River, deep water renewal, and sea floor bacterial matting. The VENUS observatory, much like the MARS location, is suited for testing equipment for other observatories due to the short distance to the sites from nearby ports. VENUS is a precursor to NEPTUNE Canada and MARS is the precursor to the RSN. NEPTUNE Canada and the RSN are both located on the Juan de Fuca Plate located off the coast of the northwestern United States [19] as shown in Figure 2. The areas for these networks were selected because of the high amount of seismic, volcanic activities, and the fact that the Juan de Fuca plate is one of the smallest tectonic plates, enabling full plate-scale experiments. NEPTUNE Canada is deployed along the northern portion of the Juan de Fuca plate and is connected to the land on Vancouver Island with data being sent to the University of Victoria for archrival purposes. The University of Victoria also hosts the data for access on the internet. Data collected from the network will be able to provide information on the activities of the tectonic plates and the surrounding ecosystems that are created in this environment. In the counterpart RSN, the network is being placed in a highly active hydrothermal vent field.

Active vent fields have many black smokers in the area that are able to support chemosynthetic life and other biological activity. When the RSN goes live, it will be able to provide continuous observation of these fields. This type of year-long, large scale observation is not possible with existing expeditions due to the limited season for ship activity and the inability for the ship to be in multiple locations at once.

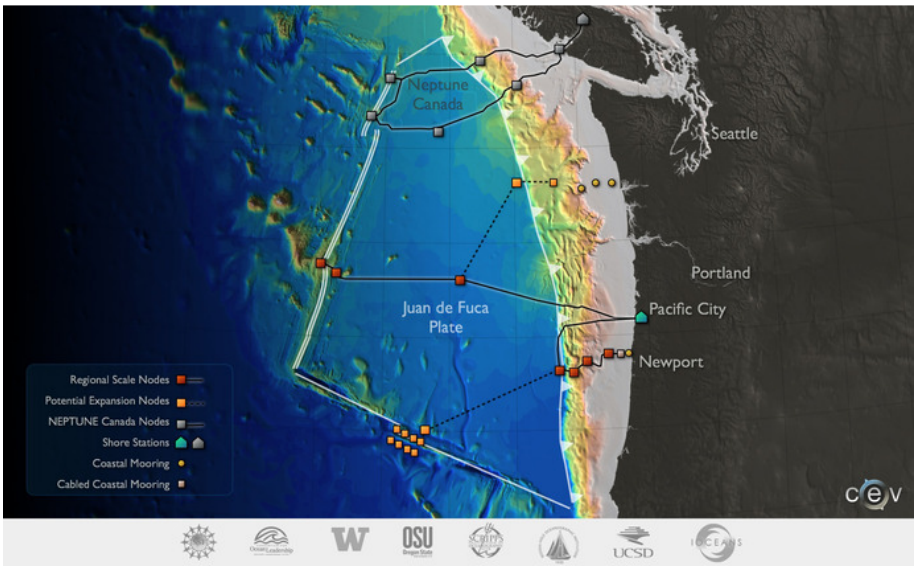

Figure 2. Placement of NEPTUNE Canada and RSN. (http://www.interactiveoceans.washington.edu/file/RSN+Plan+View, Courtesy of the OOI Regional Scale Nodes program and the Center for Environmental Visualization, University of Washington)

Another significant cabled observatory is the Defense Oceanfloor Network System for Earthquakes and Tsunamis (DONET), shown in Figure 3, located off of the southern coast of Japan near Furue-cho and operated as part of the Japan

Agency for Marine-Earth Science and Technology (JAMSTEC). The system differs from the OOI by working as an early warning system for earthquakes and tsunamis. Real-time communication to shore handled by the cable is important to allow time for preparation and emergency response for the affected areas. There is also a scientific node placed in the network, but the primary purpose is always to act as an early warning system for potential natural disasters.

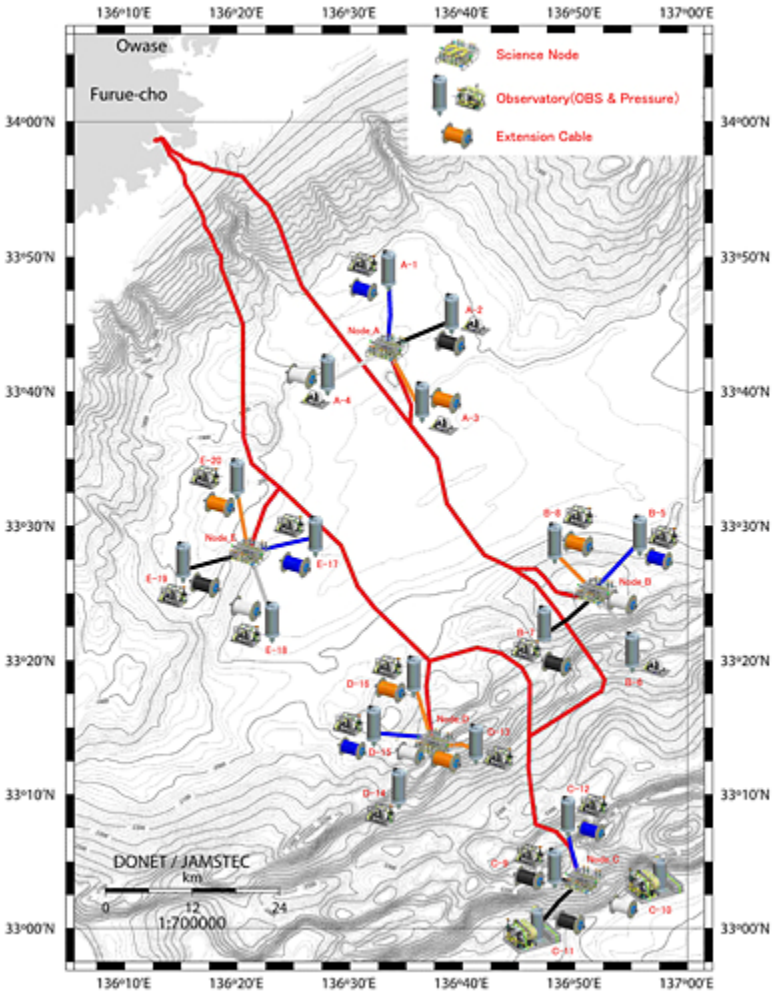

Figure 3. DONET observatory. (Courtesy of Japan Agency for Marine-Earth Science and Technology accessed at http://www.jamstec.go.jp/jamstec-e/maritec/donet/about/news/20110808/)

There are several cabled observatories not discussed in this thesis, but should be mentioned to show the wide scale adoption of underwater cabled observatories all over the world. Table 1 lists several other cabled observatories and their primary

locations. Some of these are still in development, while others have existed for many years with various purposes.

Table 1. Cabled observatories.

Sensor Network	Location(s)
MARS	Monterey Bay, CA
VENUS	British Columbia, Canada
NEPTUNE Canada	North Juan de Fuca Plate
OOI RSN	Mid-South Juan de Fuca Plate
DONET	Furue-cho, Japan
European Sea Floor Observatory Network (ESONET) [20]	Artic, Norwegian Margin, Nordic Seas, Porcupine/Celtic, Azores, Iberian Margin, Ligurian, East Sicily, Hellenic, Black Sea
Martha's Vineyard Coastal Observatory (MVCO)	South shore of Martha's Vineyard
ALOHA Cabled Observatory (ACO)	North of Oahu, Hawaii
Experimental Network for Seafloor Observatory (ENSO)	Zhejiang, China

1.2.2.2 Sensor Networks for Continual Underwater Observation

Sensor networks are comprised of sensor nodes that communicate wirelessly with each other forming an ad hoc network that eliminates or minimizes the need for onboard storage of data [21]. Many of these networks also include relay nodes, nodes that have no sensor and are only responsible for relaying information from the sensor node back to the host [22]. These networks allow real-time monitoring of a large scale area, which makes these networks ideal for long term habitat monitoring that is primarily limited by battery power [23]. Due to power constraints, sensor nodes often attempt to minimize the power

consumption with low power electronics, increasing sampling interval, and reducing the amount of data sent over the network [24].

Underwater sensor networks cannot use the same methods for continuous communication as terrestrial networks do. Terrestrial networks can accomplish continual communication by using radio frequency (rf) communication, such as Bluetooth or Wi-Fi, but rf communication is not suitable for underwater applications because of high attenuation of the signal in water [25]. One solution to underwater communication is the use of acoustics to form UnderWater Acoustic Sensor Networks (UW-ASN) [26]. These networks allow for continual monitoring of underwater environments over large areas with the primary limitation being battery power [27]. One successful network deployment completed by the University of Birmingham in Portland Harbour, United Kingdom showed communication at distances up to three kilometers [28]. Another acoustic network deployment was the Bayweb network in the San Francisco Bay completed by MBARI, Naval Postgraduate School, University of California-Berkeley, San Francisco State University Romberg Tiburon Center, and University of California-Davis / Bodega Marine Laboratory. The Bayweb network was online for 10 days with the intent of collecting real-time current observations [29]. Results from Bayweb led to the development of Seaweb. Seaweb was a network deployed on the eastern seaboard near North Carolina and was a collaboration between Naval Postgraduate School, University of Texas, US Navy Space and Naval Warfare Systems Command (SPAWAR) Systems, and

Object Video, Inc. The system was successful in detecting surface vessels that enter the area covered by the underwater network [30]. Other applications for a UW-ASN have been proposed to assist in data collection for cabled ocean observatories. Woods Hole Oceanographic Institution (WHOI) proposed using the NEPTUNE cabled observatory as the backbone of a UW-ASN. This allows for various branches of acoustic networks to be added to the cabled observatory as new regions of interest are found and the cabled observatory is expanded [31].

A second option for communication of an underwater sensor network is to use optical methods. When using optics for underwater communication, it is optimal to use wavelengths in the blue and green range because the attenuation of the light in water is lowest. A design for an optical underwater sensor network, known as Smart Plankton, has been designed and prototyped in lab tests by Anguita et al [32]. The Smart Plankton wireless sensor network is designed to consist of hundreds of small low cost sensor nodes that are capable of measuring several places in the ocean at one time. Communication is completed using the 802.11 protocol, the standard communication protocol used in Wi-Fi for laptops, modified to use blue light-emitting diodes (leds) instead of rf. By using a standardized networking protocol, existing techniques used for terrestrial networks can be extended to underwater applications [33].

1.2.2.3 Underwater Data Loggers and Data MULEs

Another option for large scale monitoring of the environment is with the use of a data logger, a device that collects data and stores it in on-board memory [34]. As opposed to the sensor network, the system is not connected in real-time, resulting in a much larger latency, but is generally able to last longer in the field due to the limited amount of power required for communication [35]. To collect the data, an automated mobile device, known as a MULE (Mobile Ubiquitous LAN Extension), is sent to the data logger [36]. The MULE collects all the data onboard the sensor and returns to the home base station to offload the data that it received from the sensor. This is also known as “muling” [37].

One successful implementation of an underwater MULE was completed at the University of Southern California [38]. The system measured temperature gradients at varying levels in a water column. Data loggers were placed at different levels in the water column. A robot submarine collects data from each data logger and returns to the surface so all the data can be retrieved for further analysis. After the data is offloaded, the submarine can have its batteries recharged and sent back to retrieve more data from the data loggers.

Another underwater MULE implementation was completed as a collaboration between the Autonomous Systems Laboratory at Commonwealth Scientific and Industrial Research Organization (CSIRO) in the Information and communication technologies (ICT) Centre in Australia and the MIT Computer Science and Artificial Intelligence Laboratory (CSAIL) [39], [40]. The system is

comprised of a sensor node, known as an Aquafleck, with a pressure sensor, temperature sensor, and a camera and a data MULE, known as Starbug [41]. Tests were completed in a swimming pool at the CSIRO AUV test facility. The Starbug was capable of successfully deploying the sensor nodes and recovering data over 46 times.

1.2.2.4 Swarm Robotics for Ocean Observation

Swarm robotics is using multiple robots to complete a single task cooperatively. This behavior can be seen in a flock of birds migrating or fish swimming in a school [42]. Flocks and schools are representative of self-organizing systems that display a collective intelligence. Using this bio-inspired model, autonomous robots could be designed to "self-organize and self-repair" [43]. These robots, though fully autonomous, are typically simple and have low levels of intelligence [44]. This simplicity of the systems often has a large amount of redundancy that prevents any single robot failure from bringing down the entire system. One example of a proposed application is to use a swarm to complete sensing of a large area [45], such as the ocean.

1.3 pH Sensing

The pH of an environment is important for monitoring the effects of acid rain and ocean acidification or for detecting biological changes that may warrant

further investigation. pH sensors can also be used to measure natural phenomenon such as the change of the pH around a black smoker on the bottom of the ocean.

There are a variety of pH sensors. Traditional glass pH probes utilize two leads and measure the potential difference: one lead measures a fixed potential and the other measures the pH-induced voltage. Glass pH probes are found in many laboratories and will be used as a gold standard for experiments discussed in this thesis. These devices are calibrated using a suite of buffer liquids with known pH values. There are also handheld devices that can be used in the field. These devices are often made waterproof and much more resistant to shock allowing them to being taken to remote field locations. Although these devices are often more rugged, they are not automated or suited for being left in the field due to the need to be regularly calibrated.

An alternative method for detecting pH is the use of optical pH sensors. One motivation for development of optical sensors is they can be placed on the end of an optical fiber and used as a probe. This is done by placing a film that fluoresces differently when placed in different pH levels. The light that is emitted is then captured by either a fiber or some other light measuring device. Many of these films adjust intensity in relation to the pH, e.g. higher pH is higher intensity and lower pH is lower intensity, or vice versa [46]. The films can have optical outputs that calibrate to either a sigmoid [47] or linear response [48]. Another form of optical sensor is the emitted wavelength changes corresponding to the pH

[49]. The detection is done by a spectrophotometer or calibrated with a photodiode that detects various wavelengths at different intensities.

There are several pH sensors that have been made for remote monitoring that are commercially available as shown in Table 2. Many of these sensors are made for aquatic environments at varying depths. Many options in performance also exist in pH range, accuracy, and response time.

Table 2. Commercially available pH sensors for field deployment.

Unit	pH Range	Accuracy	Max Depth	Response Time
WQ201 pH Sensor (Global Waters)	0 – 14 pH	2% full scale	≈18 meters	N/A
SAMI 2 (Sunburst Sensors)	7 – 9 pH	0.003 pH units	500 meters	3 minutes
pH300 (Stevens Greenspan)	0 – 14 pH	0.2 pH	N/A	2 seconds
pH sensor SBE 18 (Sea-Bird Electronics)	0 – 14 pH	0.1 pH	1200 meters	1 second
6589 pH Sensor (YSI)	0 – 14 pH	0.2 pH	60 meters	<10 seconds

1.4 Sensorbot Goals and Specifications

The goal of the thesis is to design and implement Sensorbot Beta, the first generation Sensorbot that is capable of characterizing fluorescent sensors in real-time for benchtop experiments and is capable of field deployments in shallow

water. It is necessary to characterize the fluorescent sensor because its response to different conditions is currently unknown and would allow tests to be done before making a long term deployment. The focus of the thesis will be on the design and implementation of the electrical, electro-optical and processing components to facilitate the sensor characterization. By using Sensorbot Beta, future iterations of the Sensorbot will be designed being able to take full advantage of the sensor.

The **Goals** of this thesis are to:

A. **Develop and characterize Sensorbot in a modular format.** Sensorbot Beta is a modular unit that maintains a flexible design and will significantly reduce time for improvements on the Sensorbot by allowing individual components to be improved without having to reinvent the entire unit.

B. **Characterize and calibrate sensor film on Sensorbot Beta.** A fluorescent pH sensor developed in CBDA is deposited as a thin film. The thin film is integrated with Sensorbot Beta and calibrated. An algorithm that describes the response of the sensor is used to minimize calibration time and validate the device is working properly.

C. **Evaluate Sensorbot Beta in simulated environments and complete field deployment.** Sensorbot Beta is tested in a bench top experiment with water from a local water body that will provide insight into the life time, accuracy, and response of the sensor film in real environments. Results

from this test will allow for improvement of the sensor for field deployment.

Specifications

- **Sampling Time:** Sufficiently fast sampling time to capture the dynamics of the pH sensor, which has the typical response of 10 minutes. (shown in chapter 4)
- **Signal Quality:** The noise from the signal is minimized to acceptable levels of less than three bits of noise after analog-to-digital conversion.
- **Real-time Communication:** Bench top experiments require real-time communication to a PC to alert the user if the sensor fails to respond and prevents running an entire experiment that is unnecessary.
- **Data Storage for field deployment:** Field deployments will require Sensorbot Beta to be completely standalone and will have to store approximately 2.5 megabytes of data onboard.
- **Cost:** The target budget for the components excluding the manufacturing cost is $100.00. This is an achievable cost that is low enough to maintain a cost effective unit.

2 Sensorbot Beta Hardware Design

2.1 Design Background of Sensorbot Beta

Sensorbot Beta is a testing platform for field deployable underwater Sensorbots that measures the intensity of a fluorescent sensor to measure pH changes. Sensor node designs exist for similar applications, such as a field deployable sensor node for temperature logging, which can be used to assist in the development of Sensorbot in CBDA. Although the applications and working environments of the existing sensor nodes are different from those for Sensorbots, the designs for embedded computing, data sampling and storage, and electronics are similar. A well-known miniature sensor node is the Rene Mote developed at the University of California, Berkley [50]. Rene Mote is capable of logging data from a variety of sensors. In early tests, the Rene Mote was used to detect light levels and temperature, but this could be expanded to motion and chemical sensing with the appropriate sensors. It utilizes an AT90S8535 8-bit microcontroller as the CPU, 24LC256 EEPROM as data storage, RFM TR1000 radio as the communication, AD7416 temperature sensor, and an Energizer CR2450 battery as the power source. The successor of the Rene Mote, Mica Mote [51], demonstrates the ease of improvements in the modular design. Mica Mote replaced the AT90S8535 with an ATmega128 as the CPU and improved the power source's capacity by allowing for two AA batteries [52]. Replacement of the AT90S8535 with an ATmega128 increases the RAM from 512 bytes to

4kbytes and the flash from 8kbytes to 128 kbytes. The Telos Mote, another variation of the Mote family, uses a MSP430 instead of the Atmega128. Even though the Atmega128 has a larger program memory, the MSP430 is much more conservative for power when total operation time is more important than the amount of data collected. When Motes are designed, five major categories are specified: Microcontroller type, nonvolatile storage, communication, power source, and sensor interface [53]. These five parameters will be used to lay out the hardware design of Sensorbot Beta.

2.2 Sensorbot Beta Hardware Design

Using the design parameters of microcontroller type, nonvolatile storage, communication, power consumption, and sensor interface as discussed in the previous section, the hardware of Sensorbot Beta is designed with an emphasis on a modular design format as addressed in Goal A with the use of commercial off the shelf (COTS) components to reduce cost. The block diagram of the unit is shown in Figure 4.

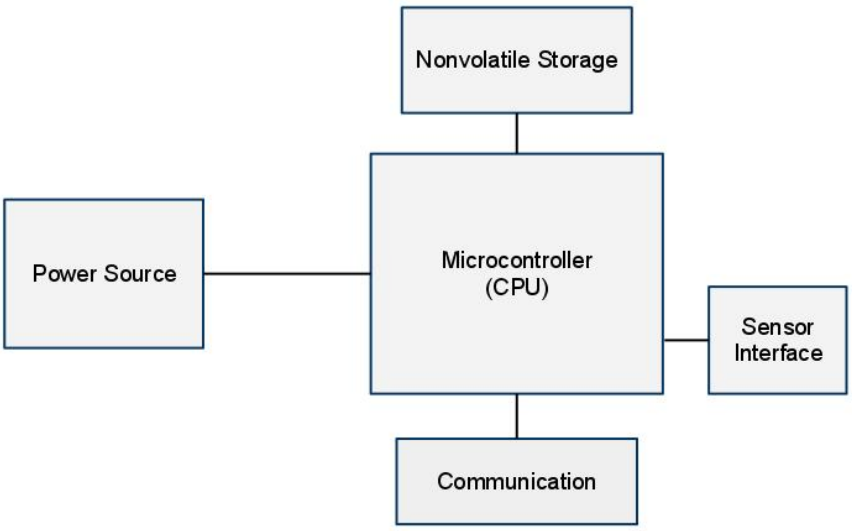

Figure 4. Core hardware of Sensorbot Beta.

2.3 Hardware Selection for Non-volatile Data Storage

Sensorbot Beta records measured data using non-volatile data storage while deployed in the field. The data is then stored until the device can be recovered and have its data offloaded. Selection of the data storage unit will determine what type of serial interface is required for the microcontroller and the operating voltage. Two different forms of non-volatile memory were considered for Sensorbot Beta, an electrically erasable programmable read-only memory (EEPROM) and a Secure Digital (SD) card, the same that is often used in portable devices. Table 3 compares the most important parameters when deciding which memory type to use.

Table 3. Non-volatile memory comparison.

	SD card	EEPROM
Storage Size	2 GByte – 32 GByte	128 bites – 1MByte
Form Factor	Standard SD card, miniSD, microSD	PDIP, TSSOP, SOIC
Communication with Microcontroller	SPI	SPI, I^2C, Microwire
Operating Voltage	2.7V – 3.6V	1.5V – 3.6V
Replacement	Remove from board	Solder
Readable by PC directly	Yes	No

In choosing the appropriate non-volatile data storage for Sensorbot Beta, it is important to understand what type of data is going to be collected. As mentioned from chapter 1, the future Sensorbot will be designed to collect pH readings in the range of minutes and be able to store the data in the field for a period of up to one year. The required storage can be estimated using Equation (2-1) assuming each pH reading is no more than five bytes.

$$\frac{5\ bytes}{minutes} * \frac{525948\ minutes}{1\ year} = 2.51\ megabytes \quad (2\text{-}1)$$

By referencing Table 3, it is clear the SD card is a better choice than the EEPROM due to the EEPROM being unable to store the appropriate amount of data. The SD card also allow for additional sampling if needed in future interactions without large modifications to Sensorbot Beta due to the ease of

replacement. For Sensorbot Beta, a two gigabyte card (Transcend Information, Taipei, Taiwan) is selected.

2.4 Hardware Selection for Communication

It is desirable to calibrate Sensorbot Beta on the bench top with real-time data acquisition. Sensorbot Beta is designed to not only store data locally on an SD card, but also have the capability to offload real-time wirelessly to a PC. Wireless communication eliminates the need of physical feedthroughs which is avoided in the design of Sensorbots, and makes the utility of Sensorbot Beta much simpler. Radio frequency (RF) communication is a well-developed solution to offload data for real-time terrestrial operations. The two potential candidates for RF communication for Sensorbot Beta were Bluetooth and Zigbee. Bluetooth was chosen over Zigbee because of the ease of use with any Bluetooth equipped computer and its ease of setup with the Bluetooth BlueSMiRF (Sparkfun Electronics, Boulder, Colorado) module. The BlueSMiRF module communicates using a standard universal asynchronous receiver/transmitter (UART) with no other setup required. This module was ideal for Sensorbot Beta due to the prototype nature of the unit.

One of the major drawbacks to using any form of RF communication on an underwater unit is that the RF is attenuated in water in several inches rendering the use of RF not possible when actually deployed. The RF communication capability of Sensorbot Beta is only designed for bench top experiments where the

amount of water is not enough to fully attenuate RF signals, but it is not suited for actual underwater deployments. One solution to this problem would be to use optical communication. Appendix B describes one option for a working optical modem that is compatible using a standard UART that was completed in CBDA with an achieved baud of 9600. Many groups have worked on development for optical underwater communication. Schill et al [54] pioneered work by using the Infrared Data Association (IrDA) standard with a LED in the blue-green spectrum to overcome the attenuation infrared in water. This work was continued at MIT's CSAIL [55], [56]. Several other groups have attempted different forms of underwater communication with various encoding methods [57–69] , but in depth discussion of these methods are outside the scope of this thesis.

2.5 Hardware Selection for the Microcontroller

The selection of the microcontroller is one of the most important selections of the entire unit because it acts as the central processing unit (CPU) of Sensorbot Beta, which is effectively the brains of the unit. It determines what components and parameters can be used with the device and sets the standard power requirements. Even though design considerations are made in the Sensorbot Beta for adjustment of the microcontroller, changing the microcontroller should only be done if necessary. When choosing the microcontroller, several considerations are made:

- The number of available Inputs/Outputs (I/O's) is important as it allows for additional sensors and other peripherals, but makes the microcontroller larger. This includes digital and analog I/O's.
- Power consumption of the microcontroller can be limiting for the device because the microcontroller is always in some form of operation mode. If the consumption is too large while idling, it can cause significant reduction of the operating lifetime of Sensorbot Beta.
- Available communication interfaces are important for peripherals and sensors, particularly Serial Peripheral Interface Bus (SPI) and Universal synchronous/asynchronous receiver/transmitter (USART) which are required for the SD card and Bluetooth.
- An onboard analog to digital converter (ADC) and its resolution should be considered for analog sensors.
- Decisions on development tools and available libraries are important when considering development time and future expansions. Considerations can also be made for a potential operating systems (OS) or standardized development tools.

The selected microcontroller for Sensorbot Beta was the 8-bit ATMEGA328P (Atmel, San Jose, California). It has SPI and USART to support the SD card and Bluetooth, respectively. An onboard 10-bit A/D converter with eight channels is available for all analog data acquisition, eliminating the need for an external ADC.

The available digital outputs will be suitable for supporting the fluorescent pH sensor described in later chapters. The operating voltage of the ATMEGA328P ranges from 1.8 volts to 5.5 volts with the idle current being around a max of 2.5mA.

One advantage of using an ATMEGA328P microcontroller is the availability of the Arduino development platform. The Arduino is an open source development platform that has several available libraries, such as a library to handle the SD card [70]. This open source system significantly reduces development time and allows for future expansion into microcontrollers with more capabilities like the ATMEGA2560 (Atmel, San Jose, California). The selected Arduino for the Sensorbot Beta was the Arduino Pro Mini (Sparkfun Electronics, Boulder, Colorado) primarily for its reduced foot print size (0.7'' x 1.3'') compared to the Arduino Uno (4'' x 2.1'') (Sparkfun Electronics, Boulder, Colorado).

2.6 Sensor Interface

As described in the selection of the microcontroller, the ATMEGA328P has analog and digital ports available. In the scope of this thesis, these are sufficient for operation of the fluorescent sensor. If higher than 10-bit resolution is desired for future expansion, an external 12-bit ADC, such as the MCP3208, could be added. Other sensors that could be added are a camera or any Inter-Integrated Circuit (I^2C) supported sensor, such as would be used to support a real-time clock.

2.7 Housing Considerations

A novel feature of Sensorbot Beta is its use of fluorescent sensors for in situ measurements and the elimination of feedthroughs for external sensors. This requires an optically clear window or housing for the sensor operations. In the design of Sensorbot Beta, a large, clear plastic test tube is used as the housing. It is large enough to house all the electronics, while being small enough as a handheld device to easily complete the field deployment. The entire electronic assembly will be kept dry inside the water-tight housing.

2.8 Software Interface

A LabVIEW interface (National Instruments, Austin, Texas), shown in Figure 5, was created to communicate with Sensorbot Beta for real-time data visualization, initialization before deployment, proper shutdown of device after deployment, deleting/creating files, offloading of data, and assistance in calibration. The interface communicates with Sensorbot Beta over Bluetooth using the PC's onboard Bluetooth card. By having a user interface with the device in real-time, calibration of the device is able to be completed much faster. It also prevents wasted time if the device calibration fails at any point in the process and allows for confirmation that the device is operating before deployment.

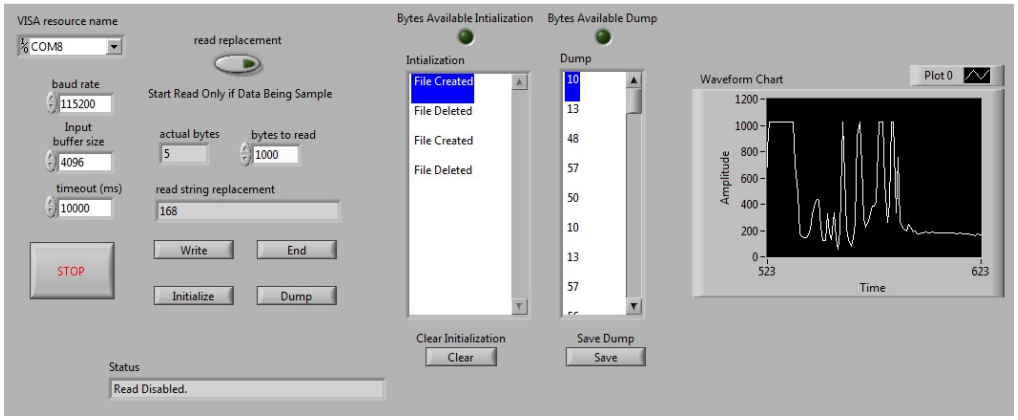

Figure 5. Sensorbot Beta Labview interface.

2.9 Length of Deployment and Size of the Unit

Operation time of the Sensorbot is a key specification for the unit. In future Sensorbot deployments, the planned operation times are at least one year. To achieve these operation times, the total amount of power on the device provided by the battery and the total power consumption of the device are two important aspects of the device. Increasing operation time requires either increasing the available power or decreasing the device's power consumption.

Total power provided to Sensorbot Beta is determined by the amount of power the battery can hold and the total amount of battery onboard. The rated battery capacity B_c can be described as

$$B_c = b_c v \qquad (2\text{-}2)$$

where b_c is the volumetric capacity and v is the volume of the battery with both of these parameters being determined from the datasheet of the battery. With the

battery capacity determined, the average constant current draw I for a certain time can be described as

$$I = \frac{B_c}{t} = \frac{b_c v}{t} \qquad (2\text{-}3)$$

where t is the total operation time. Due to the value of the battery capacity being fixed, it is clear from Eq. (2-3) that to increase operation time the total volume of the battery must be increased.

Assuming an operation time of one year (8760 hours) for the Sensorbot, the allowable constant current draw can be calculated with respects to the number of batteries required. In this calculation, Saft Li-$SOCl_2$ (0.3538 mAhr/mm^3) (Saft, Bagnolet, France) battery is chosen because of its high volumetric capacity as compared to Alkaline. The results from this can be seen Figure 6 and the linear relationship can be clearly seen. Three batteries would require an average current consumption of less than 1 mA for the year.

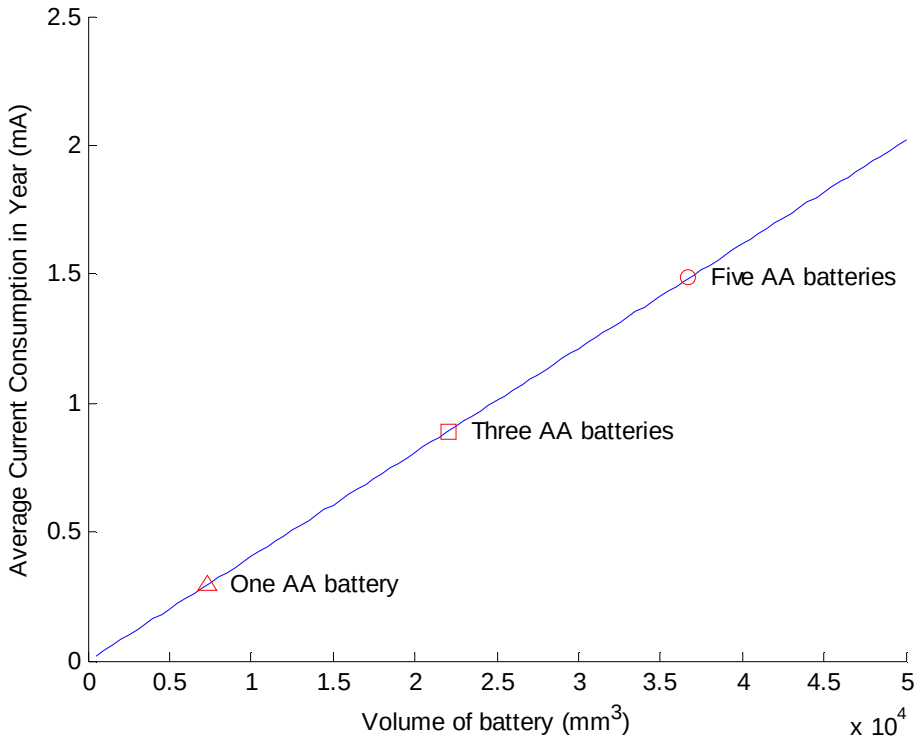

Figure 6. Average current consumption for one year of operation time.

There are two states of current draw: (1) when the Sensorbot is idling while waiting to collect data, often with an overall lower current draw, and (2) when the Sensorbot is actively collecting data, often with a higher current draw. Average current consumption is based on how often the Sensorbot is in either state. The calculation of the average constant current draw for the Sensorbot can be expressed as follows

$$I = I_{Inactive}(1 - D) + I_{Active}D \qquad (2\text{-}4)$$

Where $I_{Inactive}$ is the total current consumption when the minimum number of components is running to maintain minimum operations, I_{Active} is the current

consumption when the sensor is active, and D is the duty cycle for the Sensorbot operation. Parameters I_{Active} and $I_{Inactive}$ are measured from the power source and D can be adjusted by the user.

In the design of Sensorbot Beta, the operation time was not optimized. This is due to the prototype nature of the unit and its ability to assist in future development of the Sensorbot. For future designs, it will be important to consider operation times in relationship to the overall size of the unit.

2.10 Sensorbot Beta Implementation

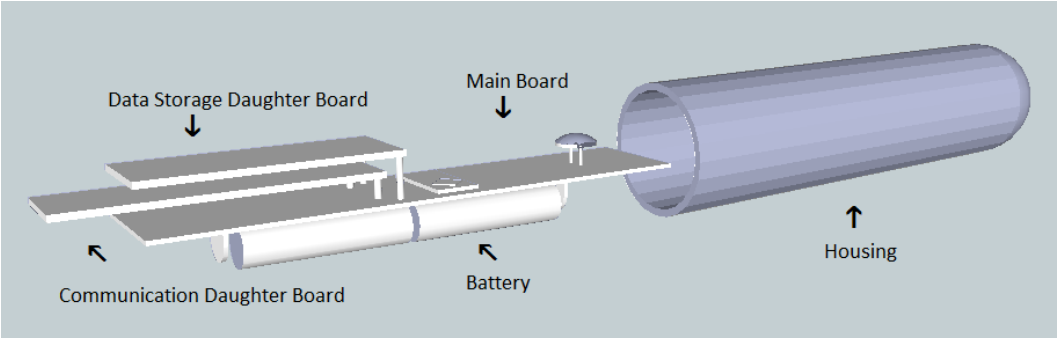

Figure 7. 3D model of Sensorbot Beta.

After the electronics for Sensor Beta are designed, a 3D model is created to assist in assembly of the device as shown in Figure 7. A custom main board holds the Arduino Pro Mini and sensor support electronics that are described later in the thesis. On the bottom of the main board, a battery holder is attached that holds two AA batteries. The SD card and Bluetooth are attached as daughter boards. The entire electronic assembly can then be inserted into the clear housing.

3 pH Sensors for Environmental Monitoring

3.1 Background of Sensor in Use

A large variety of fluorescent and phosphorescent sensors are available for many different applications. The Center for Biosignatures Discovery Automation (CBDA) in the Biodesign Institute has developed a variety of fluorescent pH and phosphorescent dissolved oxygen sensors [71]. These sensors have a wide range of biological applications on lab-on-a-chip devices [72]. With the ability to deposit the sensor in precise patterns, the sensors have proven successful for miniaturization and demonstrate the ability to perform single cell measurements to understand cellular events. The single-cell research also leads to a better understanding of the cell metabolism and its role in cancer, heart disease, stroke, and inflammation.

The aim of the thesis is to establish a platform to apply the sensors for environmental sensing. Although this application does not require microscale patterning and microfabrication, it poses new challenges that biomedical research does not have. First, unlike cell media and tissues whose pH values are typically around 7, pH values in aquatic environments are very diverse, and typically alkaline. For example, the average pH in the ocean is above 8.1, lakes in arid landscapes are very alkaline (e.g., the pH of Tempe Town Lake can reach pH 10), and the vent fluid in Lost City in the Atlantis Massif is pH between 10 and 11 [73]. The sensitive ranges of the sensors need to be adjusted. Second, the

chemistry in the environmental is diverse and the effect of salt concentration has to be characterized. Third, for long-term measurement, the durability of the sensor in the environment has to be identified.

Figure 8 illustrates the basic setup of using the sensor. An excitation source, such as a light emitting diode (LED), is used to cause the sensor film to fluoresce. The fluorescent emission will be observed by an adjacent light detector, such as a photomultiplier tube (PMT), with a filter to eliminate light from the excitation light source. In an ideal case, the filter would not be necessary because the light detector would only detect the emission spectrum of the sensor film and none from the excitation source, but in many cases this is not possible.

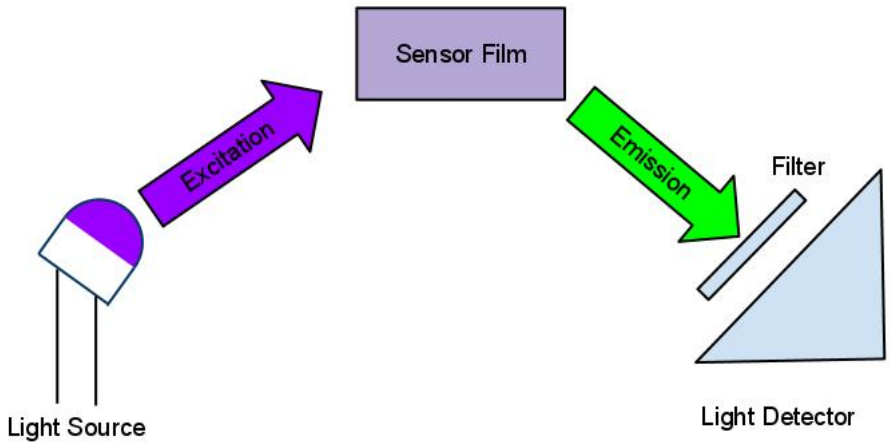

Figure 8. Basic operation of sensor.

The system developed in this thesis uses a fluorescent pH sensor, but future expansions of the system could utilize the fluorescent temperature sensors such as β-diketonate chelate europium (III), thenoyltrifluoroacetonate (EuTTA) or

a phosphorescent dissolved oxygen sensor such as platinum porphyrin. Even though the response times (i.e. lifetimes) between the fluorescent and phosphorescent sensors are multiple orders of magnitude different, the sampling time of Sensorbot Beta is 10 ms and shows no detectable difference between the sensor emissions.

The pH fluorescent sensor S1 was developed in the CBDA and operates as a fluorescent sensor as shown in Figure 8. The detailed properties of these sensors and their applications for environmental monitoring will be described in later sections. Figure 9 shows a typical absorbance spectrum (Figure 9A) and emission spectrum (Figure 9B). These plots will be used to calibrate the film and determine optical requirements of the device. The distance between the peaks of the absorption and emission spectra is the Stokes shift. As the pH increases, the emitted intensity reduces. This intensity difference is what is used to determine the pH. Also, the peak emission wavelength increases slightly, but it is not considered significant. The wavelength of peak excitation of the S1 is 405 nm and the peak emission is 510 nm varying slightly for different pHs.

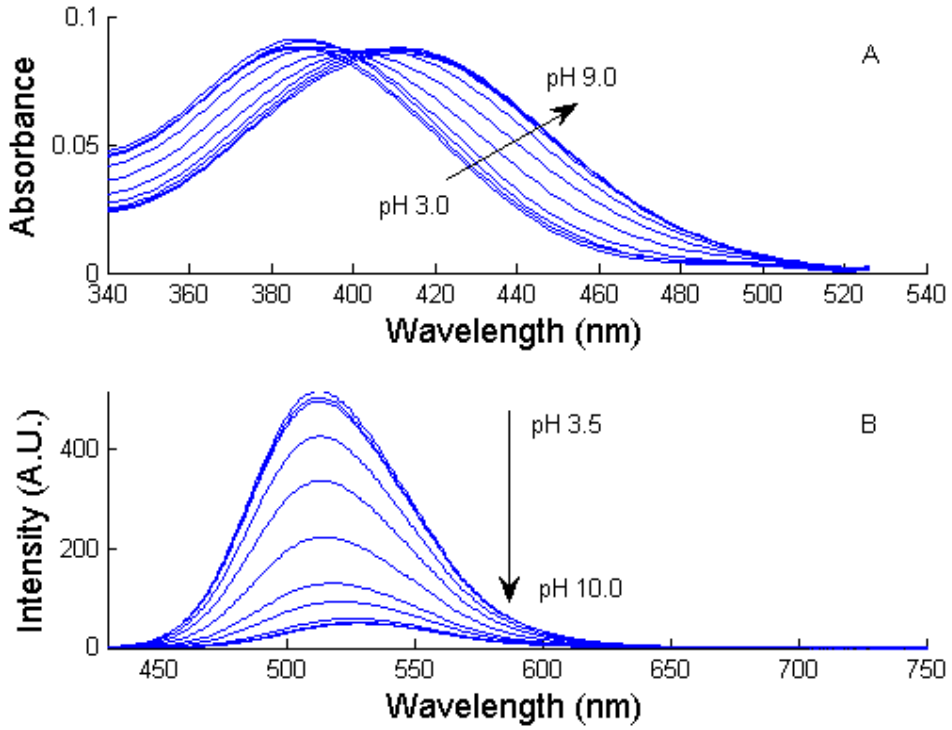

Figure 9. (A) Absorption spectrum of S1. (B) Emission spectrum of S1. (Courtesy of Dr. Yanqing Tian of CBDA.)

The relation between sensor emission and pH for S1 can be expressed as a sigmoid function

$$\frac{I}{I_0} = \frac{m_1 - m_2}{1 + e^{\left(\frac{(pH - pK_a')}{p}\right)}} + m_2 \qquad (3\text{-}1)$$

where I is the measured intensity at a given pH, I_0 is the intensity at the highest pH value, m_1 is the maximum measured fluorescent intensity, m_2 is the minimum measured fluorescent intensity and offset, pH is the pH of the solution

being measured, pK_a' is the midpoint of the sigmoid and p determines the slope of the sigmoid. Both pK_a' and p are properties of the sensor. Figure 10 is the sigmoidal function of the conventional S1 sensor that has been widely used in CBDA for biological measurements where the single-cell microenvironment is around pH 7. The blue dots are the measurements, and the red line is the calibration curve by fitting Eq. (3-1) to the measurements.

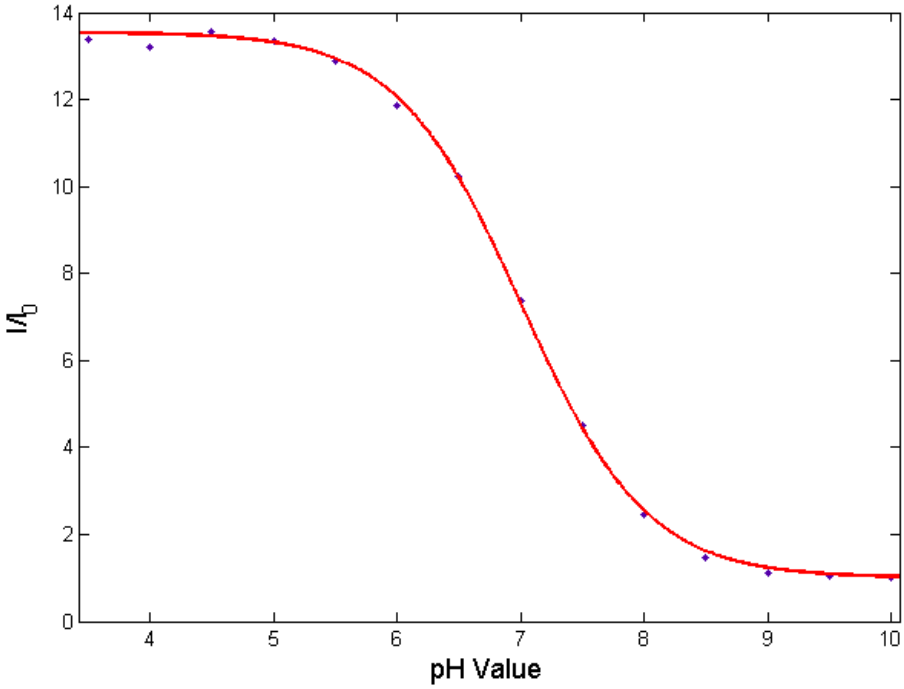

Figure 10. Calibration curve of S1 with pKa of 7.01. (Courtesy of Dr. Yanqing Tian of CBDA.)

3.2 Sensor Coating

Sensor deposition on the film is critical for effective sensing of the device. If the sensor is not properly deposited on the surface, the sensor may have

reduced intensity and longevity. In some cases, the sensor may not be functional at all.

The main steps in preparing the sensor film and depositing the sensor are to clean the film thoroughly, plasma treat the film, deposit the silane (trimethylsilylpropyl acrylate, Sigma-Aldrich St. Louis, MO) on the film using physical vapor deposition in a desiccator, place the sensor on the film, and cure in an oven. Silane is an adherent agent that facilitates permanent bonding between plastic film and pH sensor. The following provides the details of the process for preparing the sensor film.

1. Cleaning of the Sensor Film: It is important to clean the surface that the sensor will be coated on. If the film is not cleaned properly, the silane will not adhere to the surface and the sensor will begin to come off leading to the aforementioned problems. The selected film is a two mil Polyethylene terephthalate PET with adhesive on one side (Fralock Division of Lockwood Ind. Inc. Part No. T-5501-2/1 8.5 x 11.00). The films have to be cut into smaller portions allowing them to fit into a beaker. The beaker is filled with Acetone (J.T. Baker 9005-05) and DI water with a ratio of 1:1 and placed into the ultrasonic cleaner (Branson 1510) for 30 minutes. After the ultrasonic cleaning is completed, remove the film from the beaker and spray it with Acetone. The Acetone is then dried using nitrogen. It is important for the film to be completely dry before moving onto the next step.

2. Sensor Film Treatment: The process is necessary to bind silane to the PET film with the right orientation. The film is placed in the plasma cleaner (PDC-32G, Harrick Plasma, Ithaca, NY) with the surface being used for the sensor deposition, face up, for 45 minutes. The RF level should be set at medium and the pressure set at 500 milliTorr. By placing the film in the plasma cleaner, the exposed surface will be changed from hydrophobic to hydrophilic. This allows for the silane to adhere to the surface.
3. Silane Deposition: The purpose of this step is to produce a 25 µm sensor liquid on the silanized area. Take the film directly from the plasma cleaner and place it in a desiccator. The desiccator must be clean or have been used only with the specific silane. Place ten drops of silane on a kim-wipe placed in the desiccator and seal with vacuum quickly to reduce the amount of exposure for the silane. Leave in vacuum for 24 hours.
4. Slide Preparation: The sensor deposition requires a new sheet of two mil PET, two glass slides, and 25µm Kapton tapes. The new PET must be cleaned, but only needs to be washed with acetone and dried with nitrogen. After the PET is completely dried, cut the PET to fit on top of one of the slides. Using the 25 µm, tape the PET film to the slide on the edges.
5. Sensor Deposition: Cut the silanized PET to fit the slide. It is important not to touch the silanized side of the PET. This should be done quickly and the remaining film should be placed back in vacuum if intended for future use. Place the sensor on the PET film attached taped to the slide and

lay the silanized PET on the sensor with the silanized side touching the sensor. Finally, place the second slide on top of the PET.

6. Curing: The sensor is sensitive to oxygen while curing and should be in an environment with no oxygen while curing. Curing should take place at 80 °C and last for 90 minutes. This was done by using a vacuum drying oven (Yamato ADP 21). The oven is flushed with nitrogen three times and brought to a vacuum of 60 psi. After flushing, the vacuum is returned to 0 psi for curing with nitrogen filling the oven.

3.3 Testing and Calibration of Sensor

After the sensor is deposited on the PET, the film is calibrated and tested in a spectrofluorophotometer that is used as a gold standard. The spectroflourophotometer is suitable due to its high sensitivity in measuring the sensor films spectrum. It is also capable of exciting at a specific wavelength. This allows for a high accuracy of excitation and measurement of emission at a specific wavelength, typically 510 nm for the S1 sensor. Testing of the film is done by placing a piece of the sensor in a cuvette and varying the Britton-Robinson (BR) buffer. Each time the pH is changed, the previous BR buffer is removed and new BR buffer is placed in the cuvette. This allows the pK_a' and p values from Eq. (3-1) to be determined by fitting the curve to the measured data. The process involves using a set of BR buffers to measure the intensity of the sensor at several pH values.

3.3.1 S1 Sensor Film

The S1 film, as discussed previously, is a pH sensitive film that is utilized in CBDA. Figure 11 shows the calibration data gathered and the calibration curve fit to Eq. (3-1) with a $pK_a' = 8.284$ and $p = 0.4909$.

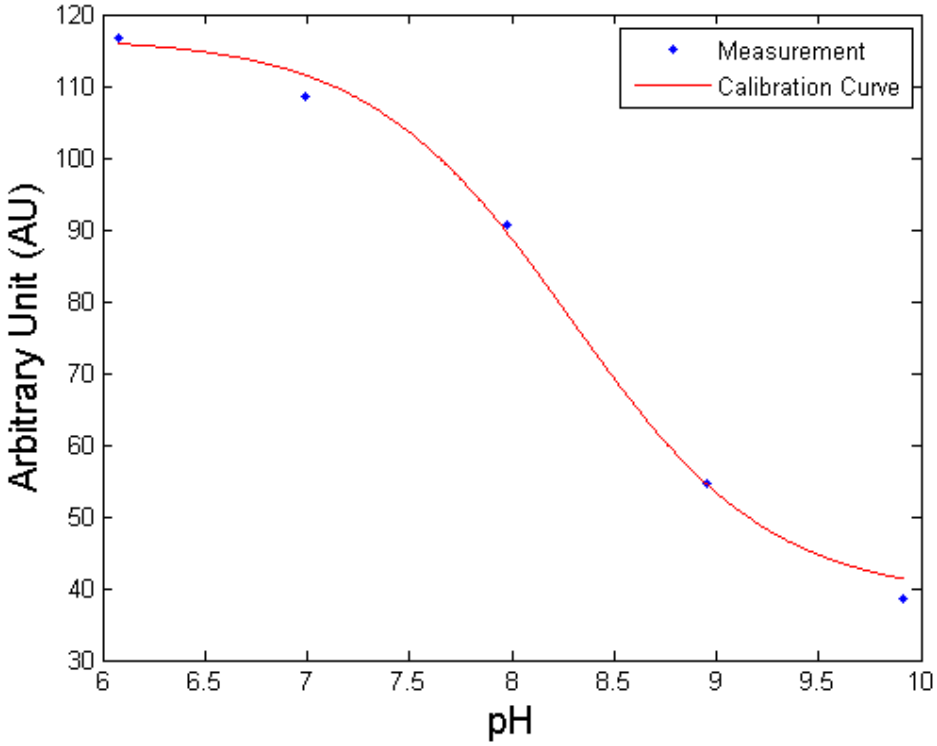

Figure 11. Calibration of S1 using spectrofluorophotometer.

3.4 S1 Optics Selection for Sensorbot Beta

By using the characteristics of the sensor described in the previous section and in Figure 9, optical components can be selected to support sensor operation

on Sensorbot Beta. Sensorbot Beta will use commercial off the shelf (COTS) components for sensor support to reduce cost, but will have less sensitivity and precision than more specialized equipment, such as the spectroflourophotometer. This requires a compromise when selecting inexpensive COTS components. Background noise may be increased due to the use of an inexpensive filter and the photodetector will be less sensitive than the expensive bench top spectroflourophotometer. The component selection will follow the components as shown in Figure 8 with an LED as the excitation light source and a photodiode as the emission light detector. A filter will be selected to cut the excitation as also shown in the figure.

As discussed earlier, the peak excitation for the S1 sensor is 405 nm and the peak emission of the S1 sensor is 510 nm with the emission beginning at 450 nm. An ultraviolet (UV) LED was selected as the excitation light source with a peak emission of 405 nm and 10% of peak emission at 436 nm. As shown in Figure 12, the spectrum of the LED is acceptable for the absorption of the sensor and does not overlap much with the emission spectrum of the sensor. The emission from the sensor is detected by a silicon PIN photodiode that has a sensitive range of 190 to 1100 nm. Due to the large sensitive range of the photodiode, a 450 nm long-pass filter is selected to cut the emission from the LED from reaching the photodiode. A small portion of the light from the LED still reaches the photodiode, as shown in Figure 12, but this is not enough to saturate the photodiode. Further analysis of the optics can be seen in Appendix A.

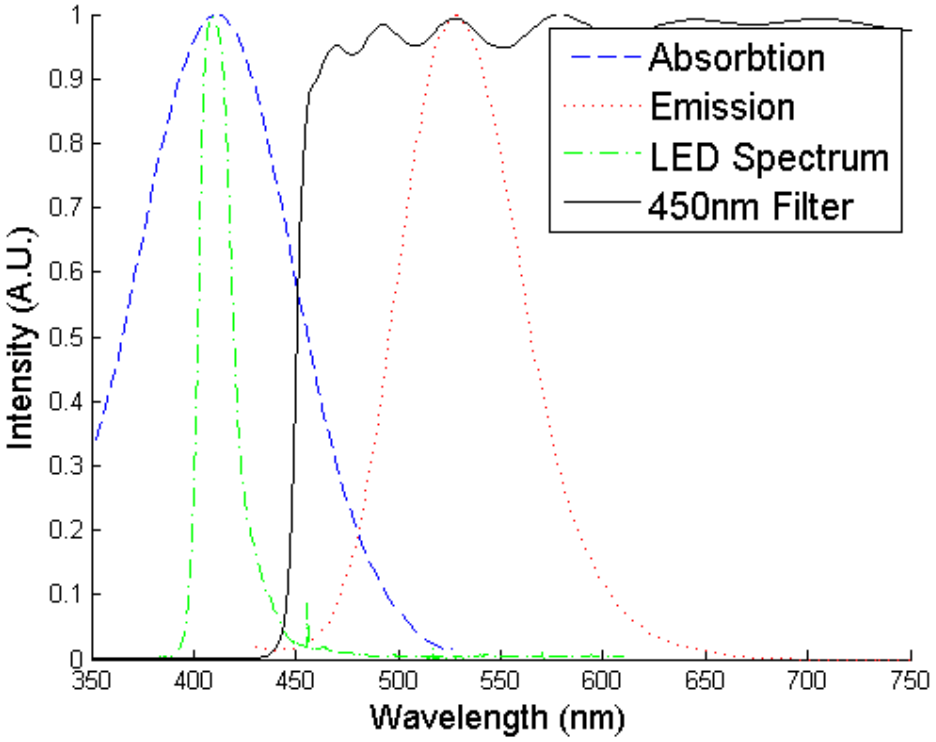

Figure 12. LED and filter selection for Sensorbot Beta.

3.5 Optics Hardware

As discussed in the previous section, the primary optical components for Sensorbot Beta are an ultraviolet LED (Bivar, Irvine, CA), silicon PIN photodiode (Advanced Photonix, Ann Arbor, MI), and a 450 nm longpass filter (Edmund Optics, Barrington, NJ). The LED is controlled directly by a digital output of the Arduino allowing the Arduino to turn the LED on and off. An analog input reads data collected from the silicon PIN photodiode. Output from the photodiode is conditioned by a transimpedance amplifier and a second operational amplifier (op-amp) to adjust the gain before going to the analog in on the photodiode. The

UA741 op-amp (STMicroelectronics, Coppell, TX) was used for both stages of signal conditioning, as shown in Figure 13, primarily for its robust characteristics and its availability in a dual in-line package (DIP) for easy replacement.

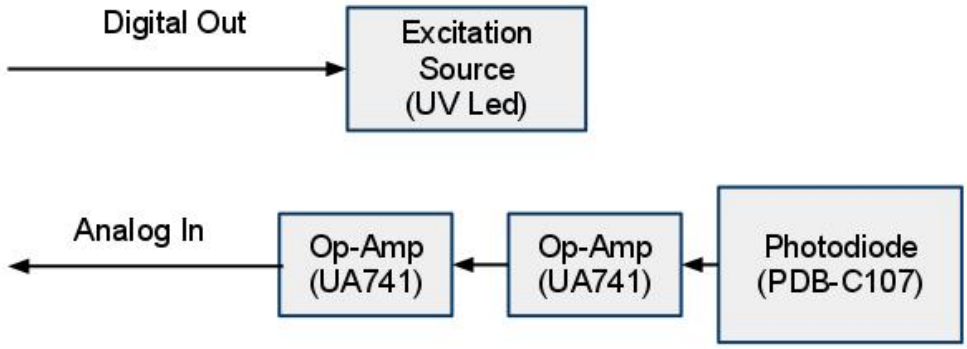

Figure 13. Sensor hardware.

3.6 Sensorbot Beta Hardware Conclusion

Using the hardware designed in chapter 2 and the optics hardware in the previous section, Sensorbot Beta electronics and sensor selection are completed. A custom board is made for the electronics according to the block diagram shown in Figure 14. Digital outputs for the LEDs are placed on pins D3 and D5 and the signal conditioned by the op-amp is connected to analog pin A2. The hardware UART pins for the Bluetooth are on pins D0 and D1. SPI pins for reading and writing the SD card are available on PIN D10, D11, D12, and D13.

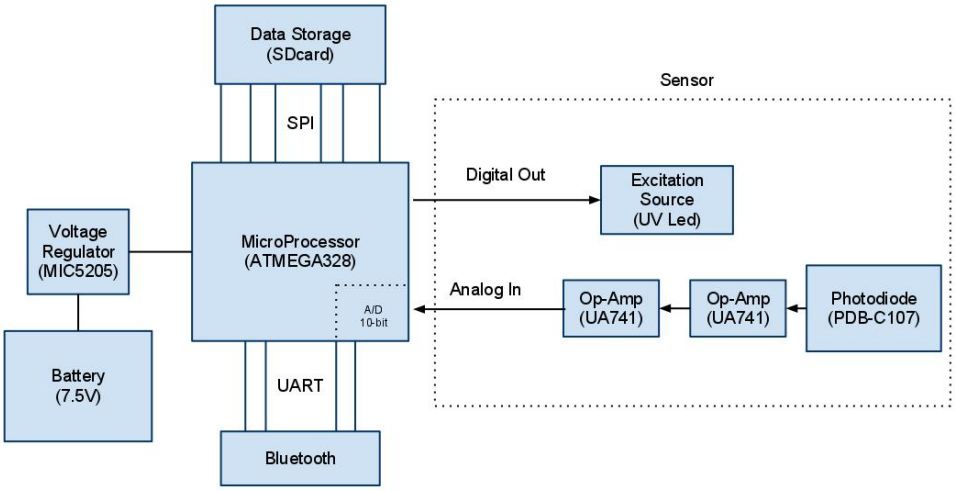

Figure 14. Sensorbot Beta complete block diagram

The cost of the components can be seen in Table 4 along with the quantity required, but does not include the cost of fabrication. Fabrication costs are excluded because in prototyping printed circuit boards are often more expensive than when placed in a final production when multiple units are produced. The total cost of components was $147.04. It is important to note that more than 50% of the cost of Sensorbot Beta was associated with the 450 nm longpass filter (NT49-025). If a more cost effective filter was selected, the goal of a $100.00 Sensorbot is obtainable.

Table 4. Cost of components for one Sensorbot Beta.

Component	Cost per Unit	Total Quantity	Total Cost
ATMEGA328P (Microcontroller)	$4.87	1	$4.87
MIC5205-5.0YM5 (voltage regulator)	$0.66	1	$0.66
Capacitors / Resistors	$1.00	1	$1.00
MicroSD Card Holder	$1.12	1	$1.12
Bluetooth	$24.95	1	$24.95
UA741CN (Op-Amp)	$0.47	2	$0.94
PDB-C107 (Photodiode)	$21.64	1	$21.64
NT49-025 (450 nm longpass filter)	$80.00	1	$80.00
VASD1-S5-D15-SIP (DC-DC Converter 5V to +/- 15V)	$5.58	1	$5.58
UV3TZ-405-30 (UV LED 405 nm)	$1.57	4	$6.28
Total Cost			$147.04

4 Sensorbot Characterization

4.1 Background

The characterization of Sensorbot Beta is important to ensure quantifiable results for field tests. This involves completing a calibration that allows for intensity values given from a sensor film to be mapped to corresponding pH values. Calibration can be completed by two methods: a full calibration using a full range of pH buffers in incremental values from the minimum intensity to the maximum intensity, or a rapid two-point calibration performed using two points near the pK_a' of the sensor. Rapid calibration will be especially important for large-scale deployment in the future to save the time for calibrating individual Sensorbots. After the calibration is completed, Sensorbot Beta can be placed in the desired aquatic environment for measurement either in a bench top experiment or a field deployment.

4.2 Full Calibration for Sensorbot Beta

The procedure for full calibration of Sensorbot Beta replicates that for the spectrofluorophotometer. A set of incremental pH values for the full range of the sensor are made using Britton-Robinson (BR) buffer that can be used to produce the sigmoid calibration curve. The values selected for the calibration of the sensor film used in this thesis range from pH 6 to pH 10 with maximum and minimum intensities, respectively. Figure 15 shows the setup of the calibration method. The

setup comprises six jars that each hold one of the pH values required for the calibration. Calibration is completed by placing Sensorbot Beta in the BR buffer for approximately 10 minutes until the film pH reading stabilizes. Premade buffers reduce a transient state when switching between pH levels. The pH values that are placed in the jars are also monitored by a conventional glass electrode to make sure the pH remains stable particularly when Sensorbot Beta is transferred in between solutions.

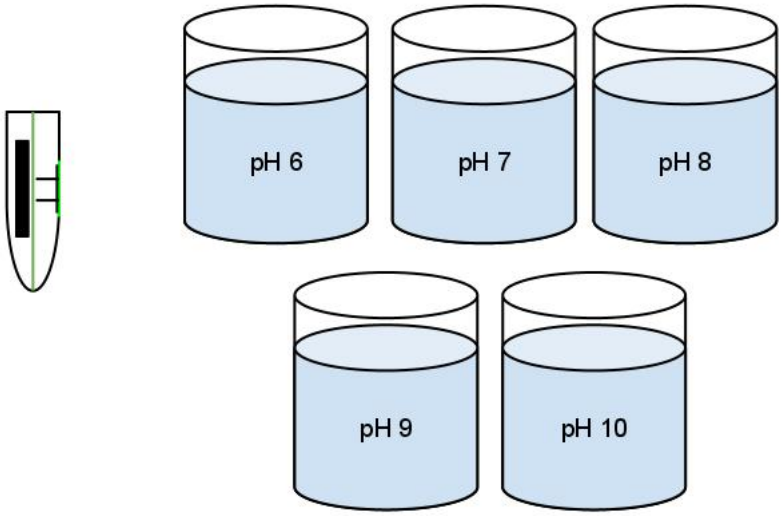

Figure 15. Experimental setup for Sensorbot Beta calibration.

After the calibration method is completed, pK_a' and p values can be determined using curve fitting for Eq. (3-1). Results from the curve fitting are shown in Figure 16 with pK_a' of 8.068 and p of 0.5721. The sigmoid curve can be used to estimate pH values from intensity values measured from the probe.

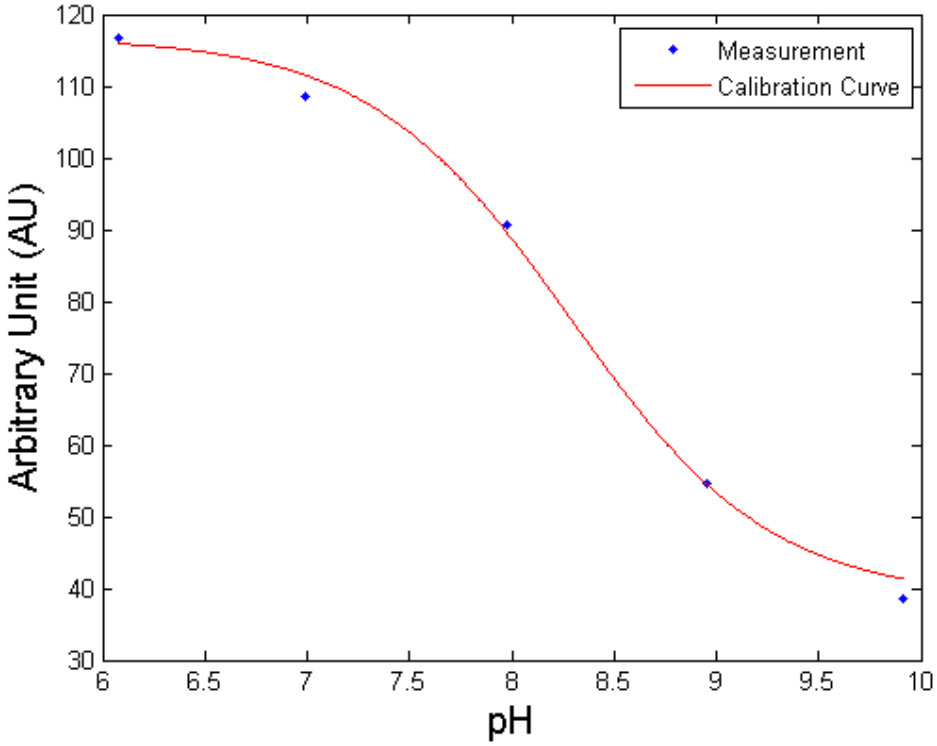

Figure 16. Calibration of pH sensor S1 with Sensorbot Beta.

4.3 Rapid Two Point Calibration for Sensorbot Beta

One of the goals of the thesis is to determine a rapid calibration method that still maintains a suitable accuracy. In the full calibration method shown in the previous section, six different calibration points are taken. Each point takes approximately 10 minutes to complete. This requires at least one hour for completion of a full calibration. By measuring only two points, the calibration time for the device can be shortened to < 25 minutes. In future iterations of the Sensorbot when several devices are deployed, it will be important to shorten the calibration time as much as possible while maintaining the accuracy.

The rapid calibration model utilizes the consistency of pK_a' and p values of the fluorescent sensor. Initial calibration of the sensor can be done using the spectrofluorophotometer to gather pK_a' and p values for the sigmoid equation as the *priori* information for rapid calibration (3-1). After these values are measured, Sensorbot Beta can do a two-point calibration using points surrounding the pK_a' in the most sensitive region. Results from this method can be seen in Figure 17 using pK_a' and p values taken from the spectrofluorophotometer calibration shown in Figure 11. The points used for calibration are the nominal pH values of 8 and 9 with the results shown in Figure 17.

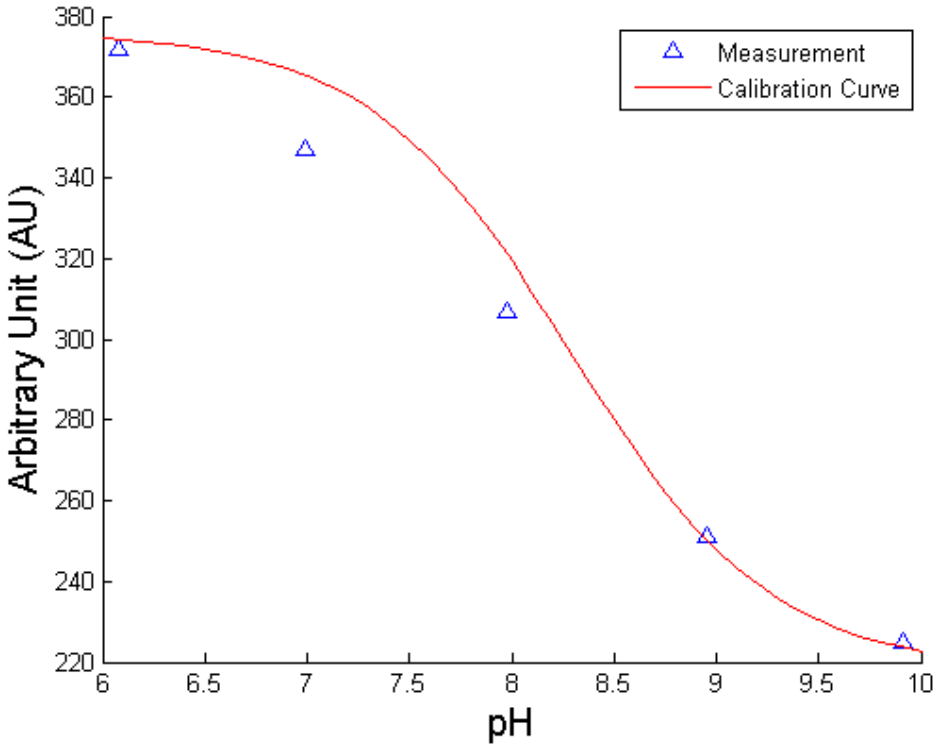

Figure 17. Calibration of pH sensor S1 with Sensorbot Beta using Two-Point Calibration.

4.4 Simulated Field Deployment

The simulated field deployment is a bench top experiment that follows that same method as the calibration shown in the previous section. A jar is filled with the desired medium, in this case lake water, and Sensorbot Beta is placed in the jar. The pH value of the measurement is derived from the sigmoid function from Equation (3-1). By rearranging the equation, the pH value of a given measured emission intensity I is

$$pH = \ln\left(\frac{m_1 - m_2}{\frac{I}{I_0} - m_2} - 1\right) p + pK_a' \qquad (4\text{-}1)$$

where m_1, m_2, and I_0 are measured during the calibration measurements stated in sections 4.2 and 4.3, pK_a' and p are calculated during calibration. Results from the test with the lake water are shown in Figure 18. The sampling rate was one sample every ten seconds. This rate ensures a sufficiently fast sampling rate to capture the dynamics of the sensors. In this experiment, the average noise of the signal was determined to be 2.16 bits after the analog-to-digital conversion with the signal strength ranging from 254 to 273 bits. This results in a signal-to-noise ratio of 126, or 42 dB, that is sufficient to detect the signal from the photodiode.

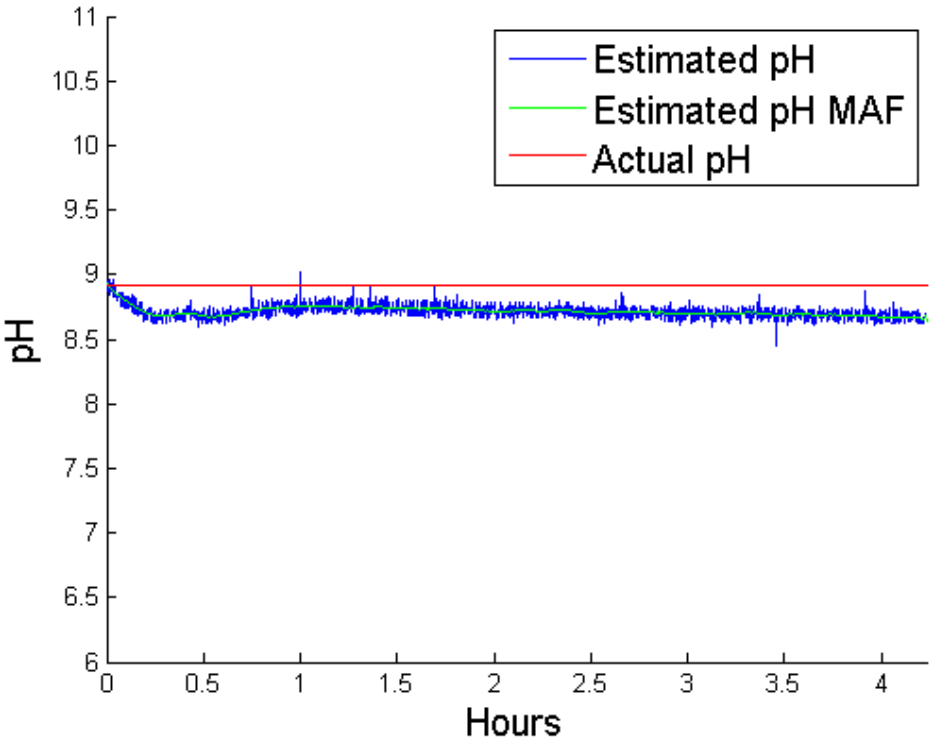

Figure 18. Benchtop Test of Lake Water with estimated pH, estimated pH with moving average filter (MAF), and actual pH.

4.5 Field Deployment

The field deployment was completed at Tempe Town Lake in Tempe, Arizona on October 17, 2011. Figure 19 shows the exact location of the deployment. This location is primarily chosen due to its close proximity to Arizona State University and it allows for easy access to the lake. The deployment location is between 12 and 14 feet deep.

Figure 19. Field test location: Tempe Town Lake, Tempe, Arizona.

The field deployment took place after sunset from approximately 6:30pm till 9:00 pm because the current Sensorbot Beta is susceptible to ambient light from the sun and the park is closed at 9:00 pm. The sampling rate was one sample every ten seconds. Actual field deployment results can be seen in Figure 20. The intensities are shown and not the pH due to the intensity values received being less than the minimum calibration values. Inspection of the figure would suggest that the sensor did not stabilize. After recovery, the sensor film would no longer respond to pH changes when placed in BR buffer, but was still physically intact, indicating that the sensor film is damaged chemically. This could have been caused by a variety factors such as an unknown chemical around the lake floor that causes the sensor to fail. Further investigation on this subject is needed. Most of the water bodies in the valley are rich in minerals and chemically manipulated

by the cities and the State of Arizona. In this experiment, the average noise of the signal was determined to be 2.13 bits after the analog-to-digital conversion with the signal strength ranging from 89 to 166 bits. This results in a signal-to-noise ratio of 78, or 38 dB.

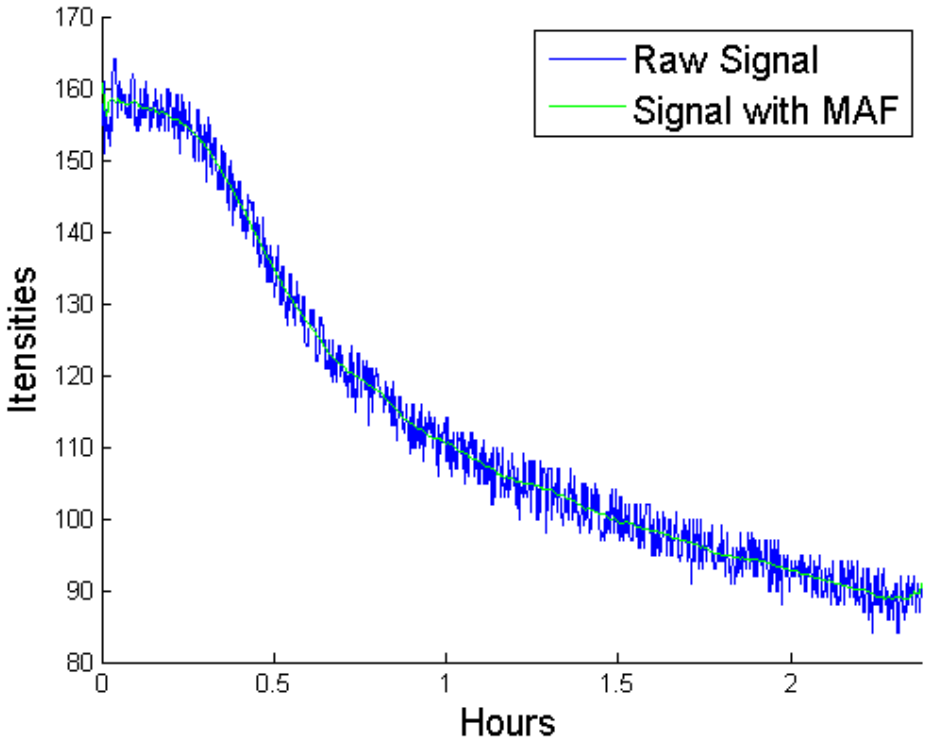

Figure 20. Field Test Results with raw signal and signal with moving average filter (MAF).

5 Conclusion

5.1 Summary of Results

A system called Sensorbot Beta was designed, built, and tested to characterize fluorescent sensors in real-time for benchtop experiments. The system is capable of field deployments in shallow water and was tested in Tempe Town Lake, Tempe, Arizona.

Sensorbot Beta is a standalone sensor node that utilizes fluorescent sensors to measure pH in situ. The data supports that the Sensorbot Beta was successful in design with the following points supporting this conclusion:

- **Modularity and Flexibility:** Sensorbot Beta maintains a modular and flexible design that is able to reduce prototyping and development time of future Sensorbot designs.
- **Cost:** The total cost of Sensorbot Beta components is $147.04 not including manufacturing costs. It is important to note that the filter has a cost of $80.00 so if a less expensive filter can be utilized, a components cost of $100 per Sensorbot Beta is possible.
- **Optics:** Calculations to determine the appropriate LED, photodiode, and emission filter for the supporting electronics of the sensor has been outlined. By having a simple outline of the required optics, the system is capable of being expanded to a variety of sensors regardless of the excitation and emission spectrum. The current

system was found to have a LED with a peak excitation of 405nm, a photodiode with sensitive range of 450nm to 600nm, and a long pass filter with a cutoff at 450nm.

- **Signal Quality:** The noise levels after the analog-to-digital conversion are constrained to be less than three bits to ensure the signal is sufficient to be read. Signal-to-noise ratios were consistently around 40 dB.
- **Characterization:** Sensorbot Beta was successfully calibrated in a bench top experiment by using incremental nominal pH values ranging from pH 6 to pH 11 that were made from BR buffer. Using the intensity values from the sensor at the corresponding pH, a sigmoid fitting was done to find a pK_a' of 8.134 and a p of 0.6105, that has a similar result to the spectroflourophotometer suggesting the calibration was successful.
- **Calibration:** A two-point calibration system was developed for rapid calibration of the pH S1 sensor on Sensorbot Beta. The pH values of the two points can be randomly selected in the operating range, but the best result is given when the two points are within the most sensitive range, which was pH 6 and pH 11 for this experiment, respectively. This result closely matches that of full calibration.
- **Simulated Field Deployment:** After completing the calibration of Sensorbot Beta, it was placed in water taken from a local water body

and was tested in a bench top setting using Bluetooth to read the intensity values of the sensor in real-time with Labview. The pH measured from a pH electrode probe was around 8.91 and the pH from the sensorbot read approximately 8.75.

- **Field Deployment:** A field test was completed in a local water body and was successfully deployed by one person. The data was stored locally on an SD card and retrieved once the deployment was completed. Results from the dive show that Sensorbot Beta was capable of measuring the fluorescent sensor and capable of operating as a standalone unit.

In summary, Sensorbot Beta was successfully developed, characterized, calibrated, and validated in a field test. Results suggest that the Sensorbot Beta with the pH sensor must be further improved to be capable of handling different environmental factors, such as salt, if the unit is to be deployed in other water bodies, such as the ocean.

5.2 Future Work

Many tasks can be done to expand upon this work, such as:

- The hardware could be improved by the implementation of high-bandwidth optical underwater communication in the form of an optical modem. Significant work has already been done in this area in CBDA and is shown in appendix A. The optical modem developed in CBDA is already capable of working with the Arduino and would

only require implementation of the hardware on the unit. With an optical modem, real-time communication could be done underwater and in the form of a sensor network. Other uses could be in the form of offloading to an AUV (autonomous underwater vehicle) and data muling back to a base station.

- The Sensorbot hardware can also be expanded to include a camera on board. A potential candidate that has been used in CBDA is the jpeg camera C328r. The C328r has been successfully used on an Arduino and is capable of storing the jpeg images to an SD card. If improvements are made on the microcontroller or a digital signal processing unit is implemented, more complex cameras can be implemented such as the OV7725 found on the SRV-1 robot.
- Precise time keeping is an important feature if units are deployed without real-time communication for extended periods of time. The onboard clock of the microcontroller can often drift and is not accurate when determining when an event occurred. Use of the DS3231 and the DS1307 would be good candidates for implementation on the sensorbot because of the support for I2C and ease of implementation with the Arduino.
- Overall lifetime of the unit can be accomplished by lowering the power requirement to 3.3 volts and the clock speed to 8 MHz for the Atmega328P. This may restrict other additions to the sensorbot, but

could act as a lower power version when lifetime of the unit is critical for the mission requirements.

- The unit may also see further miniaturization. Work on this has already been explored in CBDA. One of the primary difficulties to overcome is the battery lifetime. Units that are miniaturized will have to be capable of extreme low power operations and will need to be custom made for their mission requirements.
- Improvement in the existing data would be to measure the pH continuously using an electrode pH probe. This would require a larger testing area and an electrode pH probe that is capable of logging pH measurements without a user present. The system would allow for more rapid tests of different water types and improved rate of testing for new films.

Works Cited

[1] A. Lawlor, B. O'Flynn, J. Torres, R. Martinez-Catala, C. O'Mathuna, J. Wallace, and F. Regan, "A demonstration of wireless sensing for long-term monitoring of water quality," 2009. [Online]. Available: http://cora.ucc.ie/handle/10468/180.

[2] J. Cleary, C. Slater, C. McGraw, and D. Diamond, "An Autonomous Microfluidic Sensor for Phosphate: On-Site Analysis of Treated Wastewater," *IEEE Sensors Journal*, vol. 8, no. 5, pp. 508–515, May 2008.

[3] B. O'Flyrm, R. Martinez, J. Cleary, C. Slater, F. Regan, D. Diamond, and H. Murphy, "SmartCoast: A Wireless Sensor Network for Water Quality Monitoring," in *32nd IEEE Conference on Local Computer Networks, 2007. LCN 2007*, 2007, pp. 815–816.

[4] J. Cleary, D. Maher, C. Slater, and D. Diamond, "In situ monitoring of environmental water quality using an autonomous microfluidic sensor," 2010, pp. 36–40.

[5] Shepherd, S. Beirne, K. Lau, B. Corcoran, and D. Diamond, "Monitoring chemical plumes in an environmental sensing chamber with a wireless chemical sensor network," *Sensors and Actuators B: Chemical*, vol. 121, no. 1, pp. 142–149, 2007.

[6] E. O'Connor, A. F. Smeaton, N. E. O'Connor, and D. Diamond, "Integrating multiple sensor modalities for environmental monitoring of marine locations," 2008, p. 405.

[7] J. Hayes, G. M. P. O'Hare, H. Kolar, and D. Diamond, "Building an adaptive environmental monitoring system using sensor web," Feb-2009. [Online]. Available: http://doras.dcu.ie/4622/. [Accessed: 03-Sep-2011].

[8] G. Host, N. Will, R. Axler, C. Owen, and B. Munson, "Interactive Technologies for Collecting and Visualizing Water Quality Data," *Journal of the Urban and Regional Information Systems Association*, vol. 12, no. 3, Spring 2000.

[9] D. E. Cline, D. R. Edgington, and J. Mariette, "An Automated Visual Event Detection System for Cabled Observatory Video," in *OCEANS 2007*, 2007, pp. 1–5.

[10] W. J. Kirkwood and D. W. Caress, "Comparison of MBARI Autonomous Underwater Mapping Results for ORION Monterey Accelerated Research System (MARS) and Neptune Canada," in *Symposium on Underwater Technology and Workshop on Scientific Use of Submarine Cables and Related Technologies, 2007*, 2007, pp. 13–20.

[11] P. McGill, D. Neuhauser, D. Stakes, B. Romanowicz, T. Ramirez, and R. Uhrhammer, "Deployment of a Long-Term Broadband Seafloor Observatory in Monterey Bay," *AGU Fall Meeting Abstracts*, vol. -1, p. 1049, Dec. 2002.

[12] A. Woodroffe and A. Round, "Design and operation of a multi node cabled observatory," in *OCEANS 2008*, 2008, pp. 1–5.

[13] R. Dewey and V. Tunnicliffe, "VENUS: future science on a coastal mid-depth observatory," in *The 3rd International Workshop on Scientific Use of Submarine Cables and Related Technologies, 2003*, 2003, pp. 232– 233.

[14] C. R. Barnes and V. Tunnicliffe, "Building the World's First Multi-node Cabled Ocean Observatories (NEPTUNE Canada and VENUS, Canada): Science, Realities, Challenges and Opportunities," in *OCEANS 2008 - MTS/IEEE Kobe Techno-Ocean*, 2008, pp. 1–8.

[15] P. Fairly, "Neptune rising [undersea observatory]," *IEEE Spectrum*, vol. 42, no. 11, pp. 38– 45, Nov. 2005.

[16] S. M. Taylor, "Supporting the operations of the NEPTUNE Canada and VENUS cabled ocean observatories," in *OCEANS 2008 - MTS/IEEE Kobe Techno-Ocean*, 2008, pp. 1–8.

[17] C. R. Barnes, M. M. . Best, B. D. Bornhold, S. K. Juniper, B. Pirenne, and P. Phibbs, "The NEPTUNE Project - a cabled ocean observatory in the NE Pacific: Overview, challenges and scientific objectives for the installation and operation of Stage I in Canadian waters," in *Symposium on Underwater Technology and Workshop on Scientific Use of Submarine Cables and Related Technologies, 2007*, 2007, pp. 308–313.

[18] C. R. Barnes, "Building the World's First Regional Cabled Ocean Observatory (NEPTUNE): Realities, Challenges and Opportunities," in *OCEANS 2007*, 2007, pp. 1–8.

[19] J. Delaney, G. R. Heath, A. Chave, H. Kirkham, B. Howe, W. Wilcock, P. Beauchamp, and A. Maffei, "NEPTUNE: real-time, long-term ocean and Earth studies at the scale of a tectonic plate," in *MTS/IEEE Conference and Exhibition OCEANS, 2001*, 2001, vol. 3, pp. 1366–1373 vol.3.

[20] P. Favali and L. Beranzoli, “EMSO: European multidisciplinary seafloor observatory,” *Nuclear Instruments and Methods in Physics Research Section A: Accelerators, Spectrometers, Detectors and Associated Equipment*, vol. 602, no. 1, pp. 21–27, Apr. 2009.

[21] K. Sohrabi, J. Gao, V. Ailawadhi, and G. J. Pottie, “Protocols for self-organization of a wireless sensor network,” *IEEE Personal Communications*, vol. 7, no. 5, pp. 16–27, Oct. 2000.

[22] S. C. Ergen and P. Varaiya, “Optimal Placement of Relay Nodes for Energy Efficiency in Sensor Networks,” in *IEEE International Conference on Communications, 2006. ICC ’06*, 2006, vol. 8, pp. 3473–3479.

[23] A. Mainwaring, D. Culler, J. Polastre, R. Szewczyk, and J. Anderson, “Wireless sensor networks for habitat monitoring,” in *Proceedings of the 1st ACM international workshop on Wireless sensor networks and applications*, New York, NY, USA, 2002, pp. 88–97.

[24] M. Younis, M. Youssef, and K. Arisha, “Energy-aware routing in cluster-based sensor networks,” in *10th IEEE International Symposium on Modeling, Analysis and Simulation of Computer and Telecommunications Systems, 2002. MASCOTS 2002. Proceedings*, 2002, pp. 129– 136.

[25] Jun-Hong Cui, Jiejun Kong, M. Gerla, and Shengli Zhou, “The challenges of building mobile underwater wireless networks for aquatic applications,” *IEEE Network*, vol. 20, no. 3, pp. 12– 18, Jun. 2006.

[26] I. F. Akyildiz, D. Pompili, and T. Melodia, “Challenges for efficient communication in underwater acoustic sensor networks,” *SIGBED Rev.*, vol. 1, no. 2, pp. 3–8, Jul. 2004.

[27] E. M. Sozer, M. Stojanovic, and J. G. Proakis, “Underwater acoustic networks,” *IEEE Journal of Oceanic Engineering*, vol. 25, no. 1, pp. 72–83, Jan. 2000.

[28] K. Y. Foo, P. R. Atkins, T. Collins, S. A. Pointer, and C. P. Tiltman, “Sea trials of an underwater, ad hoc, acoustic network with stationary assets,” *IET Radar, Sonar & Navigation*, vol. 4, no. 1, pp. 2–16, Feb. 2010.

[29] S. R. Ramp, J. Rice, M. Stacey, T. Garfield, and J. Largier, “SF Bayweb 2009: Planting the seeds of an observing system in the San Francisco Bay,” in *OCEANS 2009, MTS/IEEE Biloxi - Marine Technology for Our Future: Global and Local Challenges*, 2009, pp. 1–8.

[30] J. Rice, G. Wilson, M. Barlett, J. Smith, T. Chen, C. Fletcher, B. Creber, Z. Rasheed, G. Taylor, and N. Haering, "Maritime surveillance in the Intracoastal Waterway using networked underwater acoustic sensors integrated with a regional command center," in *Waterside Security Conference (WSS), 2010 International*, 2010, pp. 1–6.

[31] L. Freitag, M. S. Ý, M. Grund, and I. Singh, "Acoustic communications for regional undersea observatories," *IN PROC. OCEANOLOGY INTL*, 2002.

[32] D. Anguita, D. Brizzolara, A. Ghio, and G. Parodi, "Smart Plankton: a Nature Inspired Underwater Wireless Sensor Network," in *Fourth International Conference on Natural Computation, 2008. ICNC '08*, 2008, vol. 7, pp. 701–705.

[33] D. Anguita, D. Brizzolara, and G. Parodi, "Building an Underwater Wireless Sensor Network Based on Optical: Communication: Research Challenges and Current Results," in *Third International Conference on Sensor Technologies and Applications, 2009. SENSORCOMM '09*, 2009, pp. 476–479.

[34] R. Mukaro and X. F. Carelse, "A microcontroller-based data acquisition system for solar radiation and environmental monitoring," *IEEE Transactions on Instrumentation and Measurement*, vol. 48, no. 6, pp. 1232–1238, Dec. 1999.

[35] Jun Luo and J.-P. Hubaux, "Joint mobility and routing for lifetime elongation in wireless sensor networks," in *Proceedings IEEE INFOCOM 2005. 24th Annual Joint Conference of the IEEE Computer and Communications Societies*, 2005, vol. 3, pp. 1735– 1746 vol. 3.

[36] R. C. Shah, S. Roy, S. Jain, and W. Brunette, "Data mules: Modeling and analysis of a three-tier architecture for sparse sensor networks," *Ad Hoc Networks*, vol. 1, no. 2–3, pp. 215–233, 2003.

[37] O. Tekdas, V. Isler, J. H. Lim, and A. Terzis, "Using mobile robots to harvest data from sensor fields," *IEEE Wireless Communications*, vol. 16, no. 1, pp. 22–28, Feb. 2009.

[38] Bin Zhang, G. S. Sukhatme, and A. A. Requicha, "Adaptive sampling for marine microorganism monitoring," in *2004 IEEE/RSJ International Conference on Intelligent Robots and Systems, 2004. (IROS 2004). Proceedings*, 2004, vol. 2, pp. 1115– 1122 vol.2.

[39] I. Vasilescu, P. Varshavskaya, K. Kotay, and D. Rus, “Autonomous Modular Optical Underwater Robot (AMOUR) Design, Prototype and Feasibility Study,” in *Proceedings of the 2005 IEEE International Conference on Robotics and Automation, 2005. ICRA 2005*, 2005, pp. 1603–1609.

[40] I. Vasilescu, K. Kotay, D. Rus, M. Dunbabin, and P. Corke, “Data collection, storage, and retrieval with an underwater sensor network,” in *Proceedings of the 3rd international conference on Embedded networked sensor systems*, New York, NY, USA, 2005, pp. 154–165.

[41] M. Dunbabin, P. Corke, I. Vasilescu, and D. Rus, “Data muling over underwater wireless sensor networks using an autonomous underwater vehicle,” in *Proceedings 2006 IEEE International Conference on Robotics and Automation, 2006. ICRA 2006*, 2006, pp. 2091–2098.

[42] C. W. Reynolds, “Flocks, herds and schools: A distributed behavioral model,” in *Proceedings of the 14th annual conference on Computer graphics and interactive techniques*, New York, NY, USA, 1987, pp. 25–34.

[43] G. Beni, “The concept of cellular robotic system,” in , *IEEE International Symposium on Intelligent Control, 1988. Proceedings*, 1988, pp. 57–62.

[44] V. Genovese, L. Odetti, R. Magni, and P. Dario, “Self organizing behavior and swarm intelligence in a cellular robotic system,” in , *Proceedings of the 1992 IEEE International Symposium on Intelligent Control, 1992*, 1992, pp. 243–248.

[45] S. Hackwood and G. Beni, “Self-organization of sensors for swarm intelligence,” in , *1992 IEEE International Conference on Robotics and Automation, 1992. Proceedings*, 1992, pp. 819–829 vol.1.

[46] T. P. Jones and M. D. Porter, “Optical pH sensor based on the chemical modification of a porous polymer film,” *Analytical Chemistry*, vol. 60, no. 5, pp. 404–406, Mar. 1988.

[47] M. J. P. Leiner and P. Hartmann, “Theory and practice in optical pH sensing,” *Sensors and Actuators B: Chemical*, vol. 11, no. 1–3, pp. 281–289, Mar. 1993.

[48] J. Lin and D. Liu, “An optical pH sensor with a linear response over a broad range,” *Analytica Chimica Acta*, vol. 408, no. 1–2, pp. 49–55, Mar. 2000.

[49] K. T. Lau, R. Shepherd, D. Diamond, and D. Diamond, “Solid State pH Sensor Based on Light Emitting Diodes (LED) As Detector Platform,” *Sensors*, vol. 6, no. 8, pp. 848–859, Aug. 2006.

[50] J. Hill, R. Szewczyk, A. Woo, S. Hollar, D. Culler, and K. Pister, “System architecture directions for networked sensors,” *SIGPLAN Not.*, vol. 35, no. 11, pp. 93–104, Nov. 2000.

[51] J. Hill, M. Horton, R. Kling, and L. Krishnamurthy, “The platforms enabling wireless sensor networks,” *Commun. ACM*, vol. 47, no. 6, pp. 41–46, Jun. 2004.

[52] J. L. Hill and D. E. Culler, “Mica: a wireless platform for deeply embedded networks,” *IEEE Micro*, vol. 22, no. 6, pp. 12– 24, Dec. 2002.

[53] J. Polastre, R. Szewczyk, and D. Culler, “Telos: enabling ultra-low power wireless research,” in *Proceedings of the 4th international symposium on Information processing in sensor networks*, Piscataway, NJ, USA, 2005.

[54] F. Schill, U. R. Zimmer, and J. Trumpf, “Visible spectrum optical communication and distance sensing for underwater applications,” *To appear in Proceedings of ACRA*, p. 1, 2004.

[55] M. Doniec, I. Vasilescu, M. Chitre, C. Detweiler, M. Hoffmann-Kuhnt, and D. Rus, “AquaOptical: A lightweight device for high-rate long-range underwater point-to-point communication,” in *OCEANS 2009, MTS/IEEE Biloxi - Marine Technology for Our Future: Global and Local Challenges*, 2009, pp. 1–6.

[56] M. Doniec, C. Detweiler, I. Vasilescu, and D. Rus, “Using optical communication for remote underwater robot operation,” in *2010 IEEE/RSJ International Conference on Intelligent Robots and Systems (IROS)*, 2010, pp. 4017–4022.

[57] W. C. Cox Jr, “A 1 Mbps Underwater Communication System Using a 405 nm Laser Diode and Photomultiplier Tube,” *Masters Thesis, North Carolina State University*, 2008.

[58] J. A. Simpson, “A 1 Mbps Underwater Communications System using LEDs and Photodiodes with Signal Processing Capability,” *Masters Thesis, North Carolina State University*, 2008.

[59] Baofeng Gao and Shuxiang Guo, “Development of an Infrared Sensor-based Wireless Intelligent Fish-like Underwater Microrobot,” in *2010 IEEE*

International Conference on Information and Automation (ICIA), 2010, pp. 1314–1318.

[60] S. Arnon and D. Kedar, "Non-line-of-sight underwater optical wireless communication network," *J. Opt. Soc. Am. A*, vol. 26, no. 3, pp. 530–539, Mar. 2009.

[61] N. Farr, A. Chave, L. Freitag, J. Preisig, S. White, D. Yoerger, and P. Titterton, "Optical modem technology for seafloor observatories," in *Proceedings of MTS/IEEE OCEANS, 2005*, pp. 928–934 Vol. 1.

[62] N. Farr, A. D. Chave, L. Freitag, J. Preisig, S. N. White, D. Yoerger, and F. Sonnichsen, "Optical Modem Technology for Seafloor Observatories," in *OCEANS 2006*, 2006, pp. 1–6.

[63] D. Anguita, D. Brizzolara, and G. Parodi, "Optical wireless communication for underwater Wireless Sensor Networks: Hardware modules and circuits design and implementation," in *OCEANS 2010*, 2010, pp. 1–8.

[64] D. Anguita, D. Brizzolara, G. Parodi, and Qilong Hu, "Optical wireless underwater communication for AUV: Preliminary simulation and experimental results," in *OCEANS, 2011 IEEE - Spain*, 2011, pp. 1–5.

[65] D. Diamond, N. E. O'Connor, A. F. Smeaton, S. Beirne, B. Corcoran, P. Kelly, K. T. Lau, and R. Shepherd, "Sensor node localisation using a stereo camera rig," in *Proceedings of the 4th workshop on Embedded networked sensors*, New York, NY, USA, 2007, pp. 43–47.

[66] M. A. Chancey, "Short range underwater optical communication links," *Masters Thesis, North Carolina State University*, 2005.

[67] J. W. Giles and I. N. Bankman, "Underwater optical communications systems. Part 2: basic design considerations," in *IEEE Military Communications Conference, 2005. MILCOM 2005*, 2005, pp. 1700–1705 Vol. 3.

[68] S. Arnon, "Underwater optical wireless communication network," *Optical Engineering*, vol. 49, p. 015001, 2010.

[69] D. Anguita, D. Brizzolara, and G. Parodi, "VHDL modeling of PHY and MAC Layer modules for underwater optical wireless communication," in *2010 5th European Conference on Circuits and Systems for Communications (ECCSC)*, 2010, pp. 185–188.

[70] S. F. Barrett and M. Thornton, *Arduino Microcontroller Processing for Everyone!* Morgan and Claypool Publishers, 2010.

[71] Y. Tian, B. R. Shumway, A. C. Youngbull, Y. Li, A. K.-Y. Jen, R. H. Johnson, and D. R. Meldrum, "Dually Fluorescent Sensing of pH and Dissolved Oxygen Using a Membrane Made from Polymerizable Sensing Monomers," *Sens Actuators B Chem*, vol. 147, no. 2, pp. 714–722, Jun. 2010.

[72] M. E. Lidstrom and D. R. Meldrum, "Life-on-a-chip," *Nat Rev Micro*, vol. 1, no. 2, pp. 158–164, Nov. 2003.

[73] M. Tivey, "Generation of Seafloor Hydrothermal Vent Fluids and Associated Mineral Deposits," *Oceanography*, vol. 20, pp. 50–65, Mar. 2007.

APPENDIX A

CALCULATIONS FOR OPTICS SELECTION

Optics design is critical for the sensor operations on Sensorbot Beta and an overview of the selection is discussed in section 3.4. Further calculations were made to confirm the results shown in Figure 12 using numerical data. In completing the calculations, three parameters are optimized:

- **Maximize the emission spectrum** by maximizing the overlap between the absorption spectrum of the sensor and the LED spectrum
- **Minimize excitation leak-through** by minimizing the overlap between the LED spectrum and the spectrum of the filter
- **Increase signal to background ratio and maximize the signal strength** by a combination of the maximizing the amount of emission from the sensor reaching the photodiode and selection of an appropriate photodiode

Maximize the emission of the spectrum

An ultraviolet LED was chosen as the excitation source with a peak emission of 405 nm and is shown matching well with the peak absorption of the sensor in Figure 12. Checking excitation sources numerically is important if more than one choice of excitation source becomes available to determine the optimal source. An ideal source would have an emission that matches the absorption spectrum of the sensor and no overlap with the emission spectrum of the sensor. This source would then maximize the amount of emission from the sensor when

excited. To determine how suitable the excitation source is for the sensor, a relation among the spectra can be expressed as

$$I_{LED}(\lambda) * I_{Absorbtion}(\lambda) = I_{TotalAbsorbtion}(\lambda) \qquad (0\text{-}1)$$

where $I_{LED}(\lambda)$ is the normalized LED spectrum as shown in Figure 21A measured by a fiber-optic spectrometer (SP1-USB Thorlabs), $I_{Absorbtion}(\lambda)$ is the sensor absorption at a specified wavelength as shown in Figure 21B for S1, and $I_{TotalAbsorbtion}(\lambda)$ is the total sensor absorption caused by the LED at the specified wavelength and should be maximized with the result in Figure 21C showing that the LED can effectively excite the sensor.

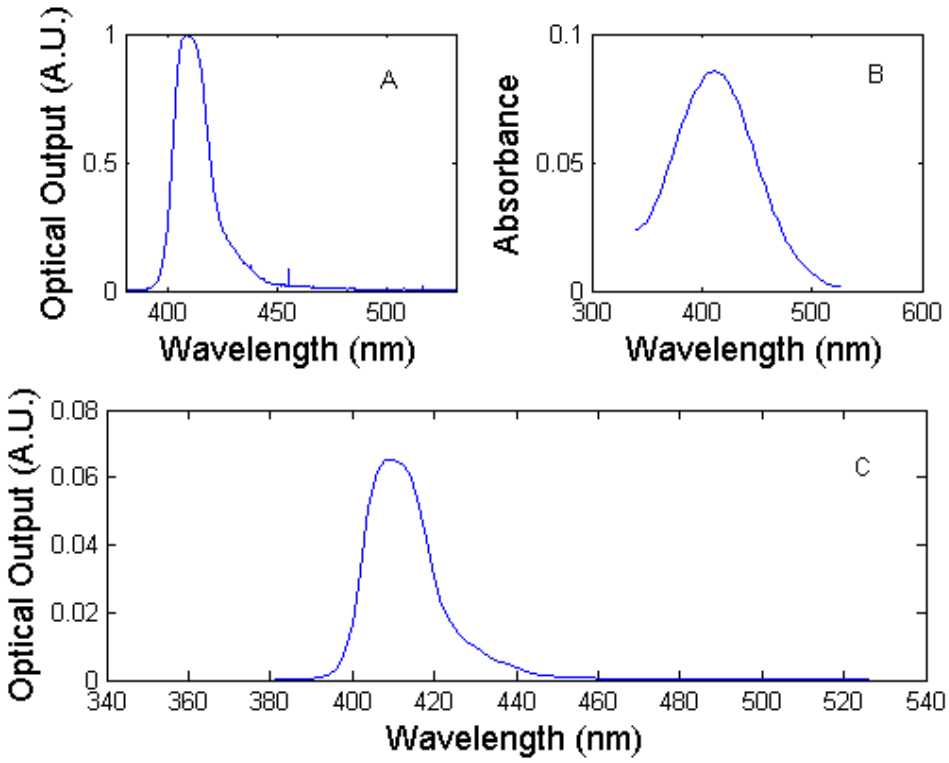

Figure 21. (A) UV LED spectrum. (B) Absorbance of pH sensor S1. (C) Sensor absorption from LED excitation for pH sensor S1.

Prevent saturation of the photodiode

The selected filter is a 450 nm longpass filter. This filter removes the excitation source from reaching the photodiode and causing saturation. As shown in Figure 12, the filter cuts a majority of the emission, but it is important to calculate the small portion that remains. Ideally, no light from the excitation source should reach the photodiode, but no filter can totally eliminate the excitation. The spectrum of light from the emission source that remains after filtering can be expressed as

$$I_{LED}(\lambda) * T_{Filter}(\lambda) = I_{LEDFilter}(\lambda) \qquad (0\text{-}2)$$

where $I_{LED}(\lambda)$ is the normalized LED output at a specified wavelength as shown in Figure 22A, $T_{Filter}(\lambda)$ is the percent transmission for the filter at a specified wavelength shown in Figure 22B as provided by the manufacturer, and $I_{LEDFilter}(\lambda)$ is the excitation from the LED after the cut from the filter as shown in Figure 22C. The term $I_{LEDFilter}(\lambda)$ should be minimized and would be zero in an ideal case. For Sensorbot Beta, less than 2% of the LED light passes through the filter.

.

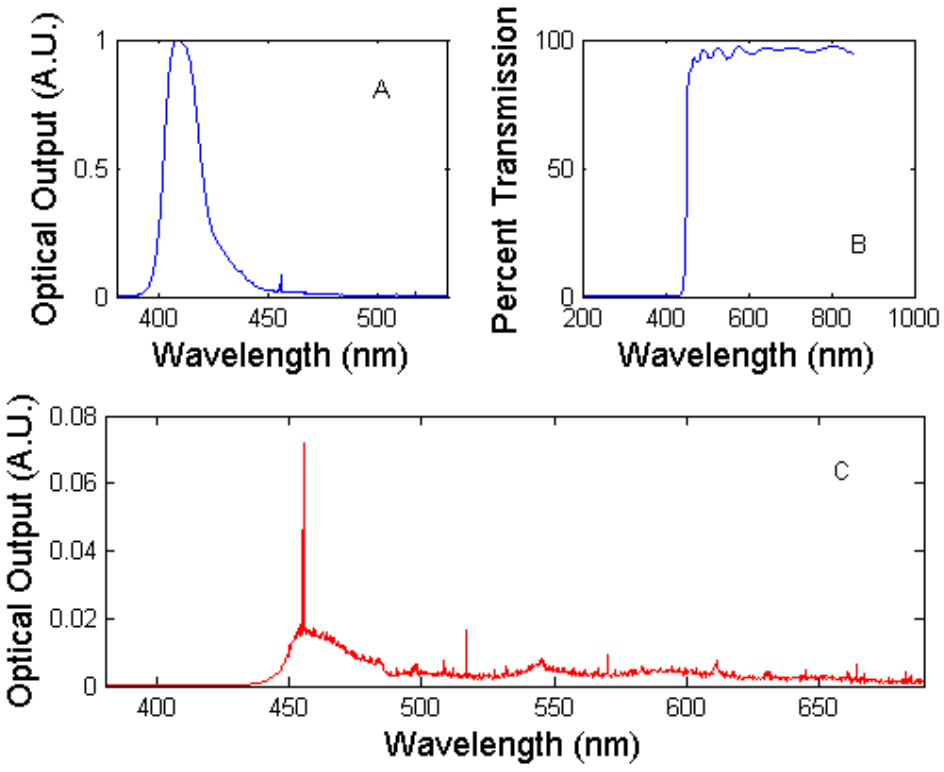

Figure 22. (A) UV LED spectrum. (B) 450nm filter transmission. (C) Excitation cut from the filter for UV LED.

Increase signal to background and maximize the signal strength

Once the filter is selected to cut the excitation, the effects of the filter should be calculated on the sensor emission. Ideally, the filter will not affect the sensor emission, but this may not be possible, especially when the Stoke shift is small. If the sensor emission after the filter is too low, a new filter needs to be selected that compromises between excitation light and emission from the sensor reaching the photodiode.

The selection of the photodiode is primarily to ensure that the photodiode is sensitive to the emission spectrum of the sensor. An ideal photodiode would only be sensitive to the emission spectrum, but not the excitation source. However, most commercially available photodiodes cover wide bandwidths, meaning that it was not possible to find a photodiode only sensitive to the emission spectrum causing the system to rely on a filter to cut the excitation source.

When selecting the photodiode, two different types of photodiode were considered, GaP and Si. The GaP generally has a wavelength spectrum of 150 to 550 and the Si is generally between 200 and 1100. Both of the photodiodes are sensitive to the emission region of the sensor. With both of the photodiode being sensitive to the excitation and emission, one of the major deciding factors was the cost of the photodiode. Si pin photodiodes cost significantly less than the GaP ones. Specifically, the PDB-C107 was chosen due to the large active area, the enhanced blue region detection, and a suitable package for placing a holder on the

filter. Another advantage of the PCB-C107 is the sensitivity to a larger spectrum in the visible region that makes the system expandable to other fluorescent sensors, such as S2, without have to change the photodiode.

Using the spectral characteristics of the filter and the photodiode, the effective signal produced from photodiode. Ideally, the emission spectrum from the sensor and signal from the photodiode would be the same. This can be numerically represented as

$$I_{Emission}(\lambda) * T_{Filter}(\lambda) * R(\lambda) = I_{Photodiode}(\lambda) \quad (0\text{-}3)$$

where $I_{Emission}(\lambda)$ is the emission of the sensor shown in Figure 23A, $T_{Filter}(\lambda)$ is the transmission for the filter in Figure 23B, $R(\lambda)$ is the spectral response of the photodiode in Figure 23C as provided by the manufacturer, and $I_{Photodiode}(\lambda)$ is the emission as viewed by the photodiode in Figure 23D. From the result, the produced signal is near the theoretical maximum in respects to the selection of the photodiode and the filter.

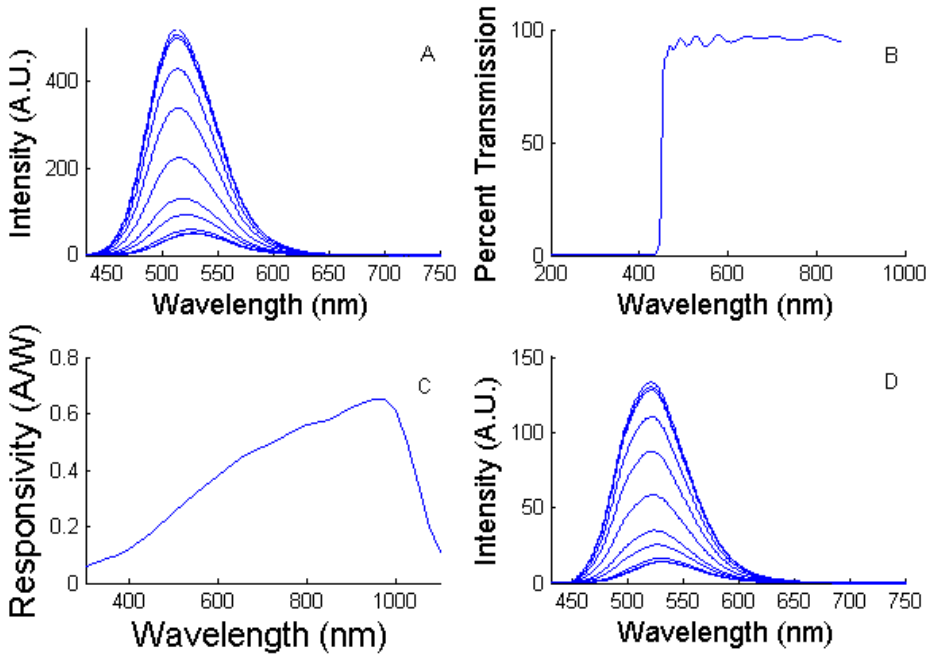

Figure 23. (A) Excitation of pH sensor S1. (B) 450nm filter transmission. (C) Photodiode spectrum. (D) Signal from photodiode.

APPENDIX B

OPTICAL COMMUNICATION

Overview of Optical Modem

The optical modem is a wireless communication system that uses an LED as the transmitter and a photo multiplier tube (PMT) (Hamamatsu Photonics, Takanawa, Japan) as a receiver. Information is encoded in the Infrared Data Association (IrDA) standard using an IC that converts the data to/from UART. In this design, an ATMEGA328 (Atmel, San Jose, CA) and PC were used, but any device that communicates using UART would be able to use the device.

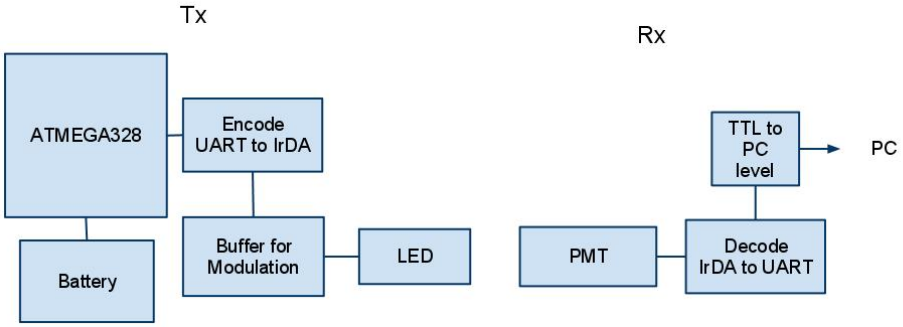

Figure 24. Optical modem overview of circuit.

An important difference between terrestrial and underwater communication is the attenuation of light in water. Existing devices use infrared LEDs for communication, hence the name of IrDA. These devices will not work underwater due to the high attenuation of infrared light underwater. A blue LED with a PMT sensitive to the blue range was chosen because blue light travels farther distances underwater than other wavelengths.

Optical Modem Circuit Design

The optical modem is broken into three components, encode/decode, transmitter (Tx), and receiver (Rx).

Encode/Decode

The unit for encoding and decoding is the MCP2120 (Microchip, Chandler, Arizona), an infrared Encoder/Decoder that supports the IrDA Physical Layer Specification. This IC encodes/decodes data from UART to IrDA and vice versa. Levels are received and sent as TTL compatible. This allows for any TTL UART compatible device to encode/decode IrDA. For the PC, a MAX232 is used to handle TTL to PC level conversions.

Transmitter (Tx)

The transmitter operates by modulating the LED. This system receives direct input form the MCP2120.

Receiver (Rx)

The receiver receives the signal using a PMT. This signal is then sent to an operational amplifier to adjust the gain. This is then output at TTL levels.

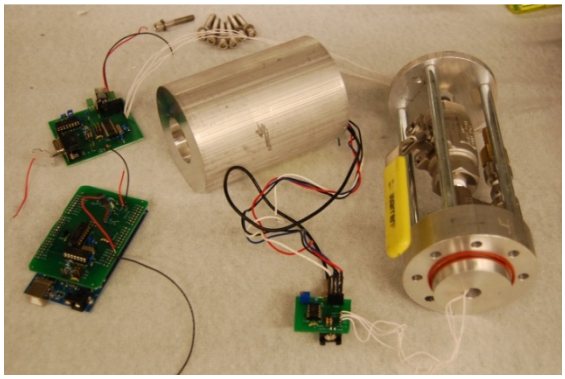

Figure 25. Picture of optical modem.

Testing the Optical Modem

The first test is to check if the modem is communicating successfully. Test strings appear are read properly and the encoding appears to be working.

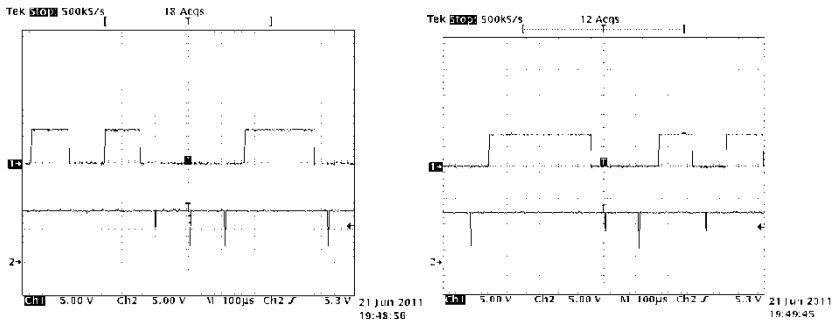

Figure 26. Output of optical modem with IrDA and UART.

Next, the optical modem is tested for successful transmission as a function of the range. A series of strings are sent to test what percentage of the strings is correctly received. This test is done as several different distances and the transmitter is continually moved back until the string can no longer be successfully transmitted.

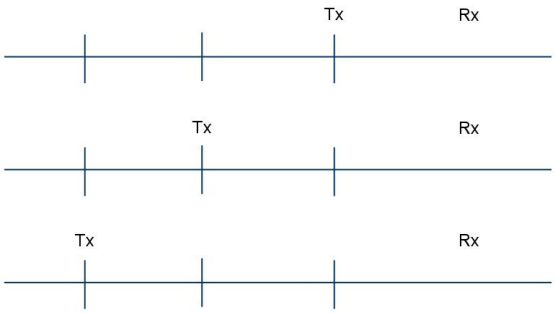

Figure 27. Test setup of optical modem.

Results from Optical Modem Testing

The results from the distance testing can be seen in Figure 28. A 100% success rate is maintained until 1.96 meters. There is considerable drop and then it returns back to a 100% success. When the same distance is tested more than once, a different result can be seen in some cases.

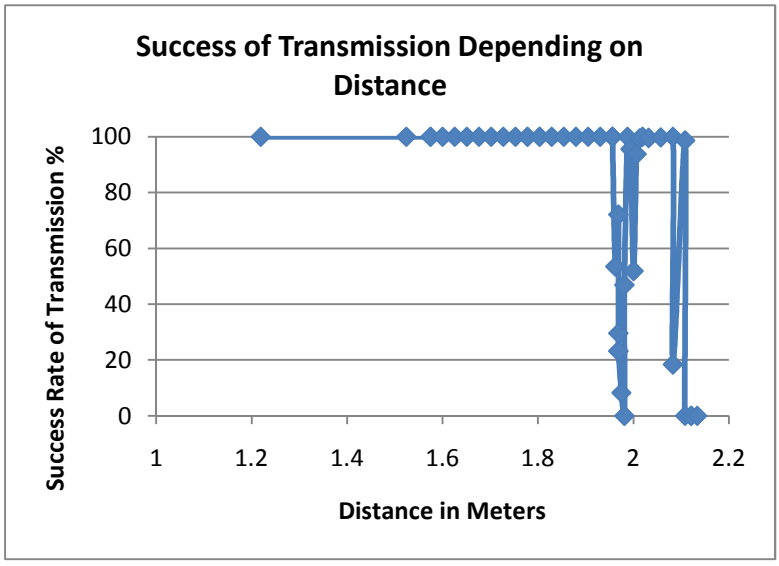

Figure 28. Results of optical modem test.